Environmental Science & Technology

pubs.acs.org/est

Article

Investigating Changes in Ozone Formation Chemistry during Summertime Pollution Events over the Northeastern United States

Madankui Tao,* Arlene M. Fiore, Xiaomeng Jin, Luke D. Schiferl, Róisín Commane, Laura M. Judd, Scott Janz, John T. Sullivan, Paul J. Miller, Alexandra Karambelas, Sharon Davis, Maria Tzortziou, Lukas Valin, Andrew Whitehill, Kevin Civerolo, and Yuhong Tian

Cite This: *Environ. Sci. Technol.* 2022, 56, 15312−15327

Read Online

ACCESS | Metrics & More | Article Recommendations | Supporting Information

ABSTRACT: Understanding the local-scale spatial and temporal variability of ozone formation is crucial for effective mitigation. We combine tropospheric vertical column densities (VCD_{Trop}) of formaldehyde (HCHO) and nitrogen dioxide (NO_2), referred to as HCHO-VCD_{Trop} and NO_2-VCD_{Trop}, retrieved from airborne remote sensing and the TROPOspheric Monitoring Instrument (TROPOMI) with ground-based measurements to investigate changes in ozone precursors and the inferred chemical production regime on high-ozone days in May−August 2018 over two Northeast urban domains. Over New York City (NYC) and Baltimore/Washington D.C. (BAL/DC), HCHO-VCD_{Trop} increases across the domain, but higher NO_2-VCD_{Trop} occurs mainly in urban centers on ozone exceedance days (when maximum daily 8 h average (MDA8) ozone exceeds 70 ppb at any monitor in the region). The ratio of HCHO-VCD_{Trop} to NO_2-VCD_{Trop}, proposed as an indicator of the sensitivity of local surface ozone production rates to its precursors, generally increases on ozone exceedance days, implying a transition toward a more NO_x-sensitive ozone production regime that should lead to higher efficacy of NO_x controls on the highest ozone days in NYC and BAL/DC. Warmer temperatures and enhanced influence from emissions in the local boundary layer on the high-ozone days are accompanied by slower wind speeds in BAL/DC but stronger, southwesterly winds in NYC.

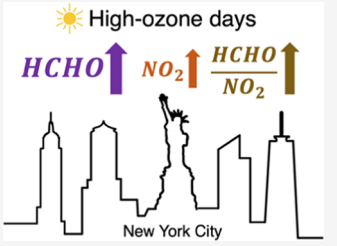

KEYWORDS: *ozone, formaldehyde, nitrogen dioxide, remote sensing, Northeastern United States*

1. INTRODUCTION

Surface ozone (O_3), a major constituent of ground-level smog, can damage the human respiratory system[1−3] and negatively affect ecosystems.[4,5] In 2015, the United States (U.S.) Environmental Protection Agency (EPA) revised the primary and secondary National Ambient Air Quality Standards (NAAQS) to a maximum daily 8 h average (MDA8) ground-level ozone concentrations of 70 parts per billion (ppb).[6] Motivated by regulations and public health, much effort has been expended to reduce ground-level ozone, but the complexity of ozone production makes mitigation a persistent challenge. We aim to improve our understanding of tropospheric ozone formation chemistry on days when MDA8 ozone exceeds 70 ppb (hereafter referred to as "exceedance days"). We focus on the northeast U.S. during the summer of 2018 (May−August) when two air quality field campaigns, the Long Island Sound Tropospheric Ozone Study (LISTOS)[7] and the Ozone Water-Land Environmental Transition Study (OWLETS-2),[8] provide a rich set of airborne and ground-based measurements of ozone and its precursors. These regional field campaigns provide an opportunity to test the capability of satellite-derived products to discerning different ozone production regimes.

New York City (NYC) and Baltimore/Washington D.C. (hereafter denoted as BAL/DC) are two densely populated regions along the Northeast Corridor that frequently exceed the ozone NAAQS.[9] Local anthropogenic[10,11] and biogenic emissions,[12,13] long-distance pollutant transport,[14−16] high temperature,[17,18] and land-water breezes over Long Island Sound[19,20] and Chesapeake Bay[21−23] have all been implicated in contributing to ozone nonattainment in our study region. Understanding ozone production and trends in NYC and BAL/DC are vital due to the large populations inhabiting the Northeast U.S. (57.6 million based on the 2020 U.S. Census Bureau estimate)[24] and may provide insights into other urban settings.

Tropospheric ozone forms when volatile organic compounds (VOCs) and nitrogen oxides (NO_x = nitric oxide (NO) + nitrogen dioxide (NO_2)) react in the presence of sunlight.[25] Sources of VOCs are diverse, including anthropogenic (e.g., from fuel combustion, solvents, and other volatile chemical products)[26] and biogenic emissions (e.g., isoprene, the dominant source in the eastern U.S. in summer).[27,28] Primary sources of NO_x include fossil fuel combustion, biomass

Received: April 27, 2022
Revised: September 7, 2022
Accepted: September 23, 2022
Published: October 11, 2022

burning, microbial activity in soils, and lightning, where the majority in the eastern U.S. in summer comes from anthropogenic sources such as road traffic and electricity-generating units (EGUs).[29] Because the ozone production rate depends nonlinearly on its precursors, ozone sensitivity to its precursor emissions is often classified into three photochemical regimes based on the primary loss pathway of odd hydrogen (HO_x) radicals.[30−33] In the NO_x-saturated regime, ozone production rates increase with declining NO_x or increasing VOCs. In contrast, ozone production increases with NO_x, while VOC changes have little impact on ozone in the NO_x-sensitive/NO_x-limited regime. Ozone production is similarly sensitive to NO_x and VOC changes in the transitional regime.[34−36]

This study uses vertical column densities (VCD_{Trop}) of formaldehyde (HCHO) and NO_2, hereafter referred to as HCHO-VCD_{Trop} and NO_2-VCD_{Trop}, as well as their ratio, which has been used to indicate the relative sensitivity of surface ozone production to emissions of VOC and NO_x.[37−40] HCHO is a commonly produced intermediate of VOC oxidation with a relatively short lifetime (∼2 h at mid-day in summer) whose spatial variability closely follows isoprene emissions over the eastern U.S. in summer and anthropogenic emissions in some urban areas.[27,41−45] Produced alongside ozone during VOC oxidation, HCHO correlates with surface ozone and even more strongly with odd oxygen ($O_x = O_3 + NO_2$).[46,47] Previous work suggests that the ratio of HCHO-VCD_{Trop} to NO_2-VCD_{Trop} (hereafter referred to as HCHO/NO_2-VCD_{Trop}) retrieved from satellite instruments can detect spatial and temporal variation trends in near-surface ozone photochemistry.[48−51] While these studies examine the long-term trends in HCHO/NO_2-VCD_{Trop}, we focus on the day-to-day variations in the ratio. We have more confidence in using the ratio to detect trends in ozone photochemistry than in determining the exact photochemical regime due to spatiotemporal variations in the threshold values that demarcate ozone production regimes and limitations in inferring surface concentrations using column densities.[49,52−54] Ozone concentrations reflect the combined impact of local photochemistry, transport (horizontal and vertical), and deposition, prompting us to examine changes in VCD_{Trop} of HCHO and NO_2 concentrations in parallel with their ratios for insights into local photochemistry conditions. We also consider the role of meteorological conditions on high-ozone versus other days.

Past climatological analyses aggregate high-ozone episodes to identify the meteorological conditions and transport patterns dominating high-ozone events.[55−58] We evaluate ozone production conditions in NYC and BAL/DC during summer 2018 from a parallel perspective by compositing measurements of ozone precursors, meteorological fields, and simulations from a Lagrangian atmospheric transport model on exceedance versus nonexceedance days. We investigate the differences in ozone precursor concentrations on ozone exceedance versus nonexceedance days and infer changes in local photochemistry. This study provides a unique perspective by aggregating different observational data products over pollution events versus other days, allowing us to detect variability not evident from simple temporal averaging, laying the groundwork for interpreting atmospheric composition retrievals from future geostationary satellites.

2. DATA AND METHODS

Data sources used in this study are listed in Table S1. We use trace gas names to refer to concentrations and explicitly state when we discuss emissions. Ozone exceedance days are defined as days on which any U.S. Environmental Protection Agency (EPA) Air Quality System (AQS) State and Local Monitoring Stations (SLAMS) (locations shown in Figure S1) in the study domain records an MDA8 ozone concentration exceeding 70 ppb (≥71 ppb). During May−August 2018, we identify a total of 22 ozone exceedance days in NYC (region defined in Figure S1b) and 17 ozone exceedance days in BAL/DC (region defined in Figure S1c) based on this criterion.

We adopt the previously derived threshold values for NYC and Washington D.C. from Jin et al.[50] to demarcate the three ozone formation regimes. Jin et al.[50] used observed ozone exceedance probabilities to identify HCHO/NO_2-VCD_{Trop} threshold values associated with the boundaries between the NO_x-saturated, transitional, and NO_x-sensitive ozone formation regimes for seven major U.S. cities. The transitional regime is identified as the top 10% of a fitted third-order polynomial curve associating the ground-level ozone exceedance probability with the Ozone Monitoring Instrument (OMI; the precursor of TROPOMI) retrieved HCHO/NO_2-VCD_{Trop}, where the exceedance probability is defined as the number of surface ozone observations exceeding 70 ppb divided by the total number of observations on all days coinciding with available VCD_{Trop} of HCHO and NO_2.[50] Given uncertainties in the exact value corresponding to a specific regime, we are most interested in the differences between exceedance versus nonexceedance days to discern relative changes in local ozone production on the most polluted days.

We use the nonparametric Wilcoxon signed-rank test,[59,60] appropriate for the non-normal distributions of HCHO-VCD_{Trop} and NO_2-VCD_{Trop}, to determine the significance of differences calculated between pairs of exceedance and nonexceedance days. Specifically, our null hypothesis assumes a distribution of these differences centered on zero. The null hypothesis is rejected if the one-sided p-value <0.01 for a median value of zero is estimated from the distribution of all differences calculated from our pairs of exceedance/nonexceedance days.

2.1. Airborne and Satellite Retrievals. We use column HCHO and NO_2 concentrations retrieved from the GEO-CAPE Airborne Simulator (GCAS) flown on the NASA LaRC B200 and Geostationary Trace gas and Aerosol Sensor Optimization (GeoTASO) flown on the NASA LaRC HU-25 Falcon aircraft during the LISTOS (June 18−October 19, 2018) and OWLETS-2 field campaigns (June 18−June 30, 2018).[7,8] GCAS and GeoTASO operate in a push-broom mode to measure backscattered ultraviolet, visible, and near-infrared (only by GCAS) light from a typical altitude of 8.5 km. These two airborne mapping spectrometers are similar, with differences in size (GCAS weighs 36 kg; GeoTASO weighs 90 kg) and spectral range (290−390 and 415−695 nm for GCAS; 300−490 and 480−900 nm for GeoTASO).[61] Further details about GCAS and GeoTASO can be found in Kowalewski and Janz,[62] Nowlan et al.,[63] Leitch et al.,[64] and Nowlan et al.[65] Judd et al.[66] provide details of these measurements during LISTOS. We use version R1 vertical column densities of HCHO and NO_2 below the aircraft (approximately the VCD_{Trop}) converted from the slant column

https://doi.org/10.1021/acs.est.2c02972
Environ. Sci. Technol. 2022, 56, 15312−15327

retrievals at a spatial resolution of 0.01° × 0.01° (Table S1). The region is sampled two to four times per flight day. The air mass factor (AMF) for column conversion is calculated using the Smithsonian Astrophysical Observatory AMF tool[65,67] following the methodology described in Palmer et al.[41] as the integrated product of the scattering weights and shape factor.[61,66−68]

During the LISTOS campaign, HCHO-VCD_{Trop} and NO_2-VCD_{Trop} retrieved from GCAS or GeoTASO are available for 12 days from June to August 2018. Seven are on NYC ozone exceedance days, and five are on nonexceedance days. We select the maximum number of available GCAS/GeoTASO flight days with sampling times closest to the TROPOMI overpass time of 1:30 PM. Our analysis uses five ozone exceedance days (2018-06-30, 2018-07-02, 2018-08-06, 2018-08-28, and 2018-08-29) and five nonexceedance days (2018-06-25, 2018-07-20, 2018-08-15, 2018-08-16, and 2018-08-24) (slashed days in Figure S2a) with the flight sampling times listed in Table S2. We do not include a parallel analysis using GCAS/GeoTASO for BAL/DC since aircraft measurements during OWLETS-2 are only available for NO_2 and only on 2 days.

We use retrievals from TROPOMI aboard Sentinel 5 Precursor (S5P) in operation since 2018 to extend our study to the entire summer (May−August). TROPOMI is a nadir-viewing shortwave spectrometer with a spatial resolution of 7 × 3.5 km^2 at nadir and daily global coverage at 1:30 PM local time.[69] Note that the improved along-track spatial resolution of 5.5 × 3.5 km^2 retrieved at nadir is only available after August 6th, 2019. We use the reprocessing stream (RPRO) version 01.01.05 L2 HCHO-VCD_{Trop} product (doi: 10.5270/S5P-tjlxfd2; access date: 8/5/2022)[70] and RPRO version 01.02.02 L2 NO_2-VCD_{Trop} product (doi: 10.5270/S5P-s4ljg54; access date: 8/5/2022)[71] re-gridded to a resolution of 0.05° × 0.05°, after selecting only pixels with quality assurance (QA) values >0.75. The QA value ranges from 0 (error) to 1 (all is well) and documents the quality of individual observations by considering cloud cover, surface albedo, geometry, and other factors. The recommended pixel filter for NO_2-VCD_{Trop} is QA > 0.75,[72] which removes errors, problematic retrievals, and cloud-covered scenes. While QA > 0.5 is recommended for HCHO-VCD_{Trop},[73] we use a stricter filter of QA > 0.75 for consistency with NO_2. Limiting the TROPOMI data to days with QA > 0.75 for both VCD_{Trop} of HCHO and NO_2 for >90% pixels in NYC or BAL/DC further restricts our analysis to 19 out of the total 22 ozone exceedance days in NYC and 10 out of 17 total days in BAL/DC.

To create as consistent a comparison as possible when comparing changes on ozone exceedance relative to non-exceedance days, we apply the same QA criterion to select a parallel set of ozone nonexceedance days, with careful attention to include similar days of the week to minimize the impact of the ozone weekday/weekend effect. In NYC, the 19 exceedance or nonexceedance days are partitioned by day of the week as: four Mondays, two Tuesdays, three Wednesdays, three Fridays, four Saturdays, and two Sundays. To minimize sampling bias, we select nonexceedance days with a similar day-of-week distribution that fall closest in time to the recorded exceedance dates. We replicate this process to identify 10 nonexceedance days in BAL/DC compared with the exceedance days: four Mondays, two Tuesdays, two Fridays, one Saturday, and one Sunday. Darker shading in Figure S2 indicates the dates used for TROPOMI analysis.

We compare the TROPOMI-retrieved HCHO-VCD_{Trop} and NO_2-VCD_{Trop} averaged separately for exceedance versus nonexceedance days. Average HCHO/NO_2-VCD_{Trop} ratios are calculated from the mean HCHO-VCD_{Trop} and mean NO_2-VCD_{Trop} on exceedance or nonexceedance days. We also conduct the same analysis using the more coarsely resolved OMI products over the NYC region (Text S1). For comparison with the LISTOS aircraft measurements, we also average the TROPOMI-retrieved HCHO-VCD_{Trop}, NO_2-VCD_{Trop}, and HCHO/NO_2 ratio only on the five exceedance versus nonexceedance days (slashed days in Figure S2a) when airborne retrievals are available.

To analyze the ozone weekend effect, we compare TROPOMI-retrieved HCHO-VCD_{Trop} and NO_2-VCD_{Trop} averaged separately for 24 Tuesdays/Thursdays and 24 Saturdays/Sundays with TROPOMI QA greater than 0.75 during May−August 2018 (Figure S3 and Text S2). We use TROPOMI retrievals to confirm that the ozone weekday/weekend effect in NYC, BAL, and DC urban centers (small regions defined in Figure S1) are distinct from the changes we find on exceedance days relative to nonexceedance days (Text S2).

We note that higher GCAS/GeoTASO HCHO-VCD_{Trop} over water is likely an artifact of the moderate resolution imaging spectroradiometer (MODIS)/bidirectional reflectance distribution function (BRDF) parametrization used for surface reflectance characterization. To avoid the impact of these errors, we remove pixels over water from the GCAS/GeoTASO retrievals. For consistency, we also remove over-water pixels from TROPOMI retrievals. We classify a pixel as over land or water using its latitude and longitude based on the version 1.0 Global Land One-kilometer Base Elevation (GLOBE) dataset (Table S1). This dataset samples the elevation of the entire earth at 1 km resolution, masking out ocean areas with a "no data" fill value of −500.[74] We define a pixel as over water if this location has a value of −500. The pixels over water are masked and removed based on the latitude and longitude grids of GCAS/GeoTASO and TROPOMI before all calculations and analysis. We only include pixels that have valid measurements (QA > 0.75 for TROPOMI and covered by aircraft flights with GCAS/GeoTASO measurements) on both exceedance and non-exceedance days.

2.2. Ground-Based Monitoring Networks. We examine surface HCHO measurements collected every five minutes during LISTOS from the EPA Office of Research and Development (ORD) Aerodyne Quantum Cascade Laser mini instrument[75] at Westport, a site along the Connecticut shoreline where ozone exceedances occur frequently. We also use hourly surface NO_2 concentrations from the SLAMS (Figure S1). The estimated measurement uncertainty is about 0.03 ppb for surface HCHO. NO_2 measurement methods and QA requirements are in compliance with EPA guidance.[76] We select measurements for the hour nearest to the TROPOMI or airborne sensors overpass time. For example, we average measurements between 1 and 2 PM as an approximation for a 1:30 PM TROPOMI overpass, and between 1 and 4 PM for a flight during 1:12−3:55 PM.

We supplement aircraft measurements with retrievals from Pandora instruments from the Pandonia Global Network (PGN) sponsored by the National Aeronautics and Space Administration (NASA) and the European Space Agency (ESA), additional Pandora instruments deployed in support of

https://doi.org/10.1021/acs.est.2c02972
Environ. Sci. Technol. 2022, 56, 15312−15327

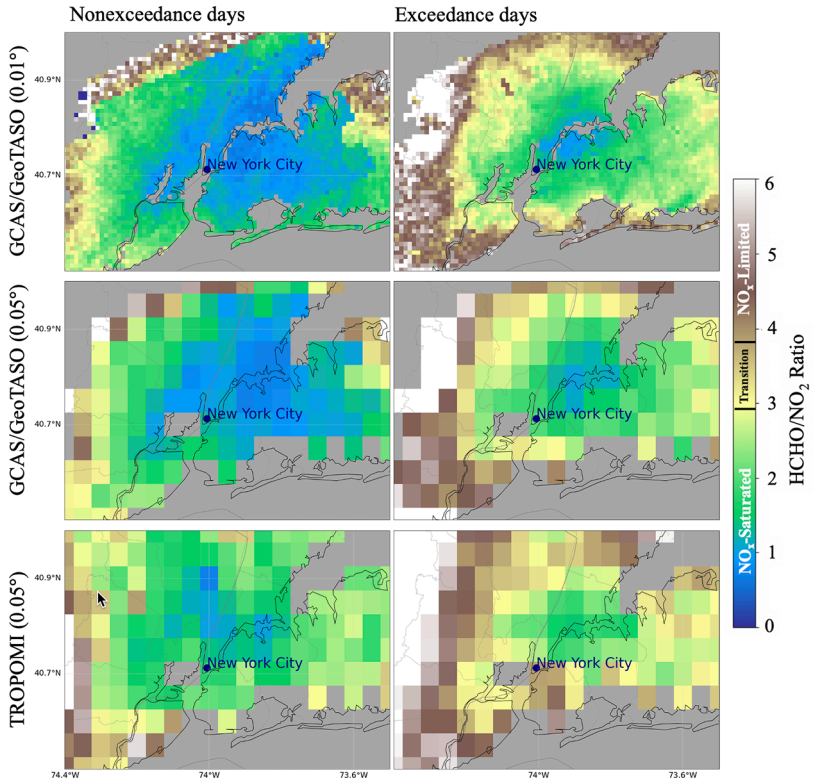

Figure 1. Areal extension of NO_x-sensitive and transitional regimes on ozone exceedance days in the New York City region. The chemical regime is diagnosed from HCHO/NO_2-VCD_{Trop} ratios, following Jin et al.,[50] as retrieved from GCAS and GeoTASO in 0.01° × 0.01° (top), re-gridded to 0.05° × 0.05° (middle), and TROPOMI in 0.05° × 0.05° (bottom) on 5 nonexceedance days (2018-06-25, 2018-07-20, 2018-08-15, 2018-08-16, and 2018-08-24; left column) and 5 exceedance days (2018-06-30, 2018-07-02, 2018-08-06, 2018-08-28, and 2018-08-29; right column) over the NYC metropolitan area during the LISTOS campaign. We only include pixels over land with measurements on both ozone exceedance and nonexceedance days; all other pixels are colored in gray.

the field campaigns, and through the Enhanced Monitoring Plans of Connecticut and New Jersey state air agencies (Table S1).[77−79] Pandora spectrometers were deployed at 10 sites during LISTOS: Rutgers (NJ), Bayonne (NJ), Manhattan (NY), Queens College (NY), Bronx Pfizer (NY), Flax Pond (NY), Westport (CT), New Haven (CT), Hammonasset (CT), Outer Island (CT) (Figure S1a); and at three sites during the OWLETS-2 campaign: Earth System Science Interdisciplinary Center (ESSIC), the University of Maryland Baltimore County (UMBC), and Hart-Miller Island (HMI), all in Maryland (Figure S1c).[80,81] The Pandora instruments are ground-based ultraviolet−visible spectrometers that can operate in direct-sun and sky-scan mode to retrieve O_3, NO_2, sulfur dioxide (SO_2), HCHO total columns, tropospheric columns, and vertical profiles.[82−85] We do not use HCHO columns from the Pandora spectrometers due to sensor off-gassing-induced errors in the current 2018 products.[86] Trace gas abundances along the light path are determined using differential optical absorption spectroscopy (DOAS). The estimated error in the Pandora retrievals of total VCDs of NO_2 (NO_2-VCD_{Total}) is approximately 1.35 × 10^{15} molecules/cm^2.[87] We filter NO_2-VCD_{Total} following Tzortziou et al.[84] and estimate NO_2-VCD_{Trop} by subtracting the TROPOMI NO_2 stratospheric VCDs (NO_2-VCD_{Strat}) from the Pandora NO_2-VCD_{Total} (Text S3). We examine NO_2-VCD_{Trop} measured by the Pandora spectrometers for the hour surrounding the TROPOMI overpass time (around 1:30 PM local time) for the entire summer (19 exceedance days versus 19 nonexceedance days) to allow sufficient data for comparison.

2.3. Continuous Emission Monitoring Systems (CEMS) NO_x Emissions, Meteorology, and Transport.

We use hourly NO_x emissions recorded by continuous emission monitoring systems (CEMS) that estimate NO_x emissions based on reported operations from a large subset of power generation and industrial sources.[88] We calculate average NO_x emissions for 24 h and mid-day (10 AM to 2 PM) time spans summed for all monitored power plant units in NYC (42 total) and BAL/DC (22 total) on ozone exceedance and nonexceedance days as well as on Tuesdays/Thursdays and Saturdays/Sundays for our weekday/weekend analysis. The locations of power plants within and near NYC and within BAL/DC are shown in Figure S1.

We contrast meteorological conditions using 2 m above ground temperatures and 10 m above ground winds from Phase 2 of the North American Land Data Assimilation System (NLDAS-2) derived from the North American Regional Reanalysis (NARR).[89] We use the version 002 hourly level-4 primary forcing data product with a spatial resolution of 0.125° × 0.125° (Table S1). We calculate the average of the 1 and 2 PM local time to coincide with the TROPOMI overpass (around 1:30 PM). We also examine day-by-day wind maps to show that the average wind patterns are not dominated by a small number of days. We use the Stochastic Time-Inverted Lagrangian Transport (STILT) model driven by NOAA High-Resolution Rapid Refresh (HRRR) meteorology at 3 km horizontal resolution (together referred to as HRRR-STILT), as a relative indicator of the influence of surface emissions on

https://doi.org/10.1021/acs.est.2c02972
Environ. Sci. Technol. 2022, 56, 15312−15327

Table 1. Change on Exceedance Days Relative to Nonexceedance Days[a]

Change on exceedance days relative to nonexceedance days Nonexceedance → Exceedance				
	$\Delta HCHO$	ΔNO_2	$\Delta(HCHO/NO_2)$	Percentage of Pixels in (NO_x-Saturated, Transitional, NO_x-Sensitive)
NYC (5 days; 0.01° × 0.01°; 2983 pixels)	**+96%**	**+4%**	**+144%**	**(81, 8, 11) → (52, 18, 30)**
NYC (5 days; 0.05° × 0.05°; 125 pixels)	**+96%**	**+4%**	**+62%**	**(81, 10, 9) → (53, 18, 29)**
NYC (5 days; 137 pixels)	+66%	+4%	+63%	(80, 13, 7) → (28, 33, 39)
NYC (19 days; 137 pixels)	+79%	+36%	+35%	(81, 16, 3) → (52, 28, 20)
BAL/DC (10 days; 840 pixels)	+13%	+5%	+5%	(2, 4, 94) → (0, 0, 100)

[a]We only include pixels with QA > 0.75 for TROPOMI or covered by aircraft flights with GCAS/GeoTASO measurements on both exceedance and nonexceedance days. Relative changes in HCHO-VCD_{Trop}, NO_2-$VCD_{Trop,}$ and $HCHO/NO_2$ on exceedance days (left three columns; see Figure S2 for date classifications, Figure S1b for NYC, and Figure S1c for BAL/DC), and the percentage of pixels in each region where the $HCHO/NO_2$-VCD_{Trop} falls into each chemical regime for ozone formation using the values derived from Jin et al.[50] for the New York City (NYC), Baltimore (BAL), and Washington D.C. (DC) regions, respectively (right column). Retrievals are from TROPOMI except in bold for airborne sensors (GCAS or GeoTASO). Shaded values indicate Wilcoxon signed-rank tests with a p-value <0.01, suggesting that the difference between exceedance and nonexceedance days are significant (distribution of the differences is not centered at zero).

ozone concentrations at selected locations on exceedance versus nonexceedance days (Text S4).

3. OZONE EXCEEDANCE VERSUS NONEXCEEDANCE DAYS

3.1. New York City. Our analysis excludes pixels that are over waterbodies or have retrievals only on exceedance or nonexceedance days (gray pixels in Figure 1). Table 1 shows changes in regional averaged HCHO-VCD_{Trop} NO_2-VCD_{Trop}, and $HCHO/NO_2$ ratios on ozone exceedance days relative to nonexceedance days and the percentage of pixels classified as NO_x-saturated, transitional, and NO_x-sensitive based on Jin et al.[50] Differences with a p-value <0.01 for a one-sided Wilcoxon signed-rank test are shaded (Table 1). We find increases in HCHO-VCD_{Trop} and NO_2-VCD_{Trop} in NYC from both airborne GCAS/GeoTASO (+96 and +4%, respectively) and TROPOMI satellite retrievals (+66 and +4%, respectively) on high-ozone days during the LISTOS campaign (Table 1 and Figures S4 and S5). TROPOMI satellite retrievals for May–August 2018 in NYC also show enhanced VCD_{Trop} of both species (+79 and +36%, respectively; Figure S6). The TROPOMI enhancement in NO_2-VCD_{Trop} on ozone exceedance days is more significant during the summer (p-value <0.01) versus during the LISTOS campaign (p-value = 0.1 for GCAS/GeoTASO and TROPOMI). To test the significance of the differences detected on the flight days, we randomly select and compare TROPOMI HCHO-VCD_{Trop} and NO_2-VCD_{Trop} on five exceedance versus five nonexceedance days from the 19-day exceedance/nonexceedance pairs over the entire summer. This comparison suggests that these 10 flight days are representative of the differences from nonexceedance to exceedance days during summer 2018 (Text S5 and Figure S7). We do not find a distinct rural–urban gradient in HCHO-VCD_{Trop}, whereas NO_2-VCD_{Trop} is consistently higher in the NYC urban core.

Figure 1 shows $HCHO/NO_2$-VCD_{Trop} ratios averaged over 5 nonexceedance days (left) and averaged over 5 exceedance days (right), from GCAS and GeoTASO at 0.01° × 0.01° (top), at 0.05° × 0.05° (middle), and TROPOMI in 0.05° × 0.05° (bottom) for the dates and flight times specified in Figure S2 and Table S2. For NYC, Jin et al.[50] diagnosed the

https://doi.org/10.1021/acs.est.2c02972
Environ. Sci. Technol. 2022, 56, 15312−15327

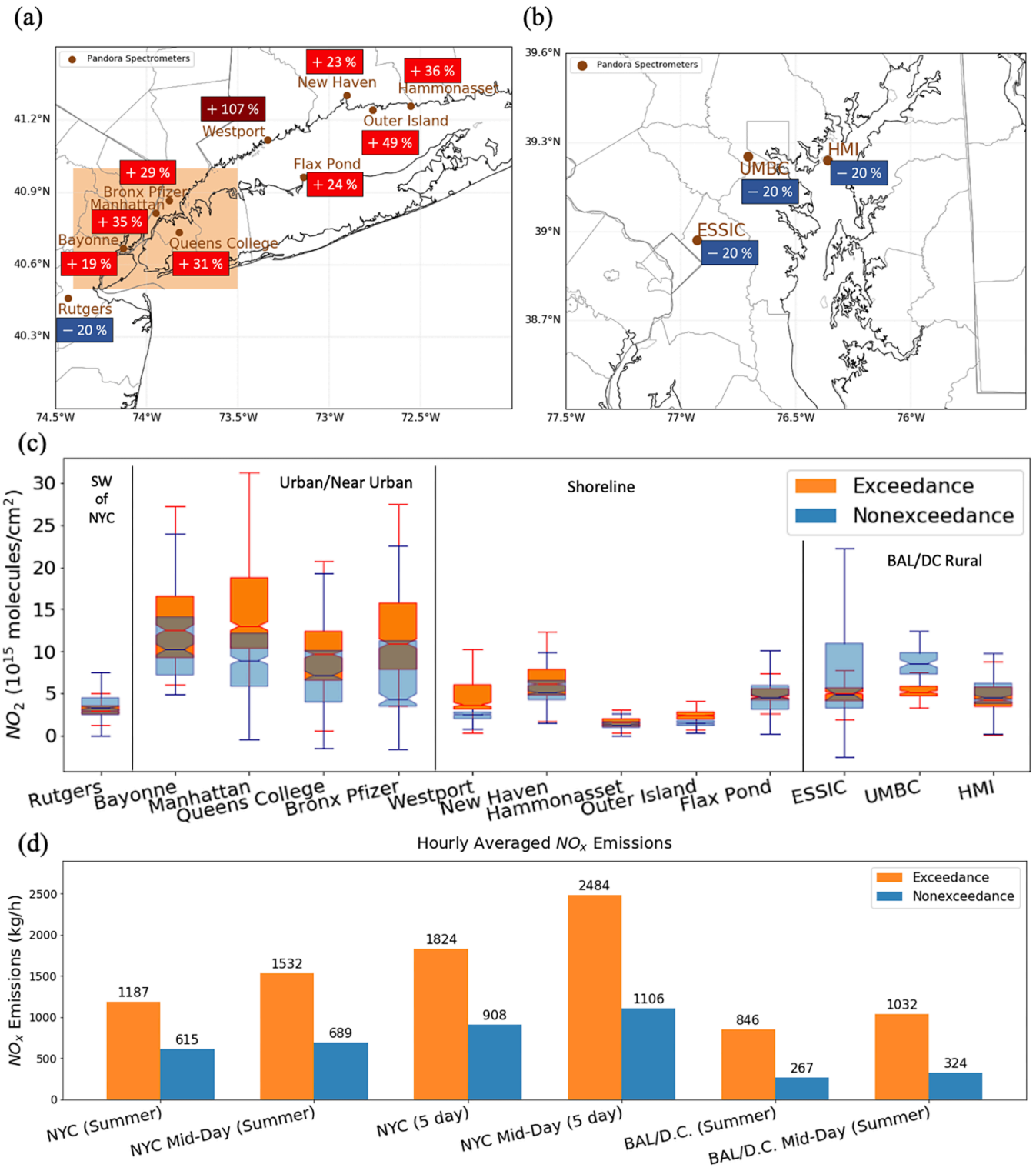

Figure 2. Higher NO_2-VCD_{Trop} at four urban sites near NYC and along the shoreline but lower NO_2-VCD_{Trop} at Westport and three suburban BAL/DC sites on high-ozone days during summer 2018, along with higher power plant NO_x emissions in NYC and BAL/DC. Changes in averaged Pandora NO_2-VCD_{Trop} estimated at 1:30 PM for the entire summer on exceedance days relative to nonexceedance days site in (a) NYC and (b) BAL/DC. (c) Box plots for NO_2-VCD_{Trop} measured by the Pandora spectrometers extending from the 25th to the 75th percentile, with a line at the median and a whisker showing the range of the data. (d) NO_x emissions from EGUs monitored by continuous emission monitoring systems (CEMS) are higher on ozone exceedance days in both NYC and BAL/DC. We calculate hourly averaged NO_x emissions for 24 h and mid-day (10 AM to 2 PM) periods, summed for 42 power plant units in NYC and 22 units in BAL/DC on exceedance (orange), and nonexceedance days (blue).

transitional regime as occurring when HCHO/NO_2-VCD_{Trop} ratios range from 2.9 to 3.8, with ratios below this range indicating NO_x-saturated ozone formation and above indicating a NO_x-sensitive regime. We apply these values to infer

https://doi.org/10.1021/acs.est.2c02972
Environ. Sci. Technol. 2022, 56, 15312−15327

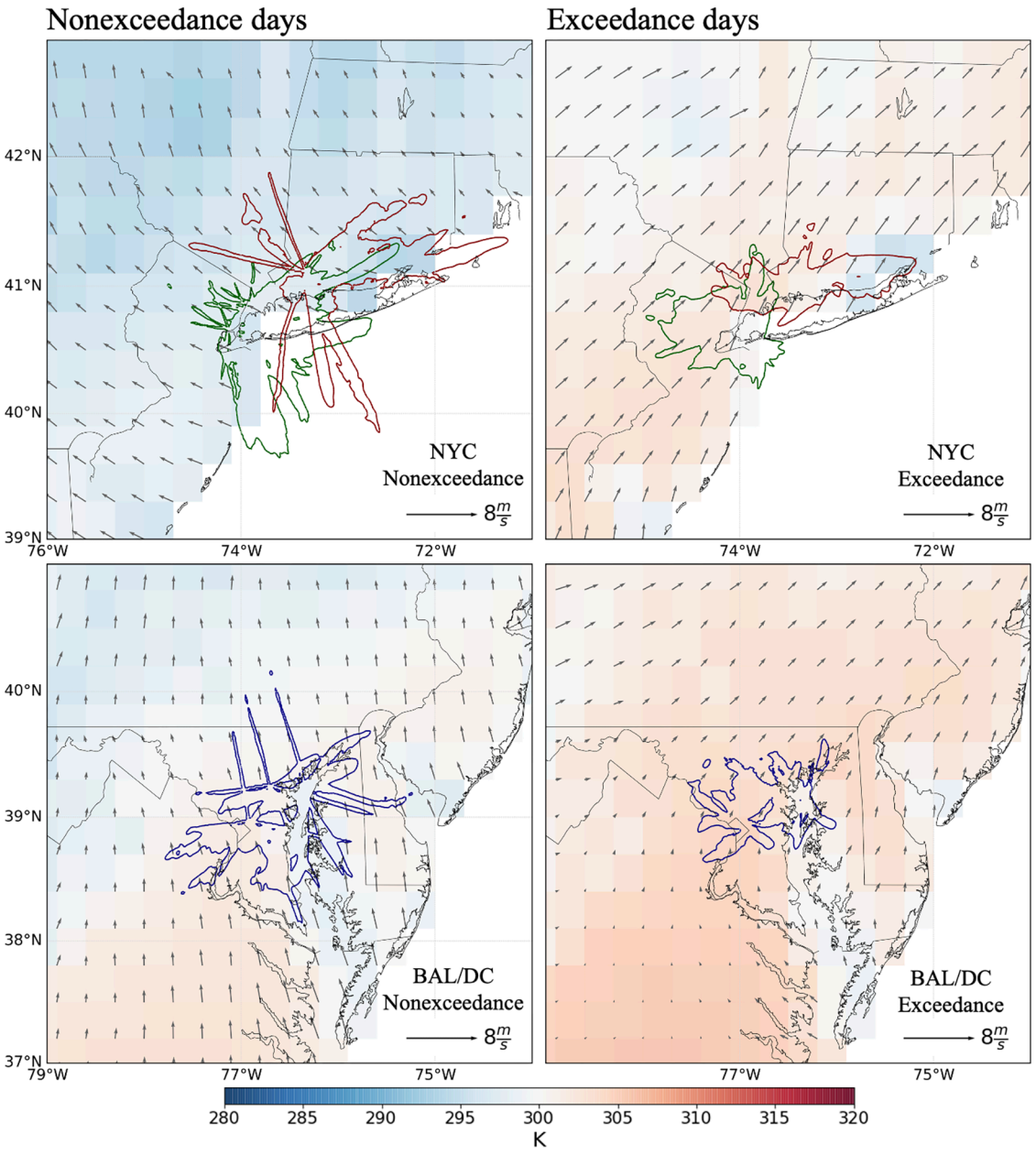

Figure 3. Higher temperatures and stronger winds occur on ozone exceedance days in NYC, but weaker winds co-occur with ozone exceedance and warmer temperature days in BAL/DC, with a greater impact from local ozone sources on exceedance days in both regions. Shown are 0.01 ppb (μmol m^{-2} s^{-1})$^{-1}$ contour lines from the mean HRRR-STILT footprint that represents the summed 6 h surface influence on concentrations at 50 m above ground level for the Pandora site at Westport (Figure S1a; red), four sites near NYC (Figure S1b; green), and three sites in BAL/DC (Figure S1c, blue). The 2 m above ground temperature and 10 m above ground wind from NLDAS-2 estimated at 1:30 PM averaged for 19 nonexceedance (upper left) and 19 exceedance (upper right) days in NYC and 10 nonexceedance (bottom left) and 10 exceedance (bottom right) days in BAL/DC are re-gridded to 0.3° by 0.3° resolution to improve wind arrow legibility.

shifts in the ozone production regime from the ratios. On exceedance days, changes in HCHO-VCD$_{Trop}$ dominate and higher HCHO/NO$_2$-VCD$_{Trop}$ ratios occur over a larger area in NYC. The rural−urban HCHO/NO$_2$-VCD$_{Trop}$ gradient in Figure 1 agrees with previous findings of less NO$_x$-sensitive regimes in urban areas relative to the surrounding suburbs.[38,90] The regional mean HCHO/NO$_2$-VCD$_{Trop}$ ratios on the 5 exceedance- versus nonexceedance days increase by 62% for the re-gridded aircraft and 63% for TROPOMI retrievals (Table 1 and Figure 1). On the 19 exceedance versus nonexceedance days, the regional mean TROPOMI HCHO/NO$_2$-VCD$_{Trop}$ ratio increases by 35% (Table 1 and Figure S6). For the 19-day comparison, OMI suggests similar qualitative changes in HCHO-VCD$_{Trop}$ and NO$_2$-VCD$_{Trop}$ as TROPOMI, although the ratio only increases for the pixels closest to NYC urban center (Text S1 and Figure S8). The more coarsely resolved OMI products (0.25° × 0.25° versus 0.05° × 0.05° for TROPOMI) miss the fine-scale spatial changes and indicate a greater enhancement in HCHO-VCD$_{Trop}$ and NO$_2$-VCD$_{Trop}$ than either the TROPOMI or GCAS/GeoTASO retrievals.

The tropospheric column increases in Figures 1, S4, and S5 over NYC from nonexceedance to exceedance days are consistent in sign with the changes in the surface measurements of HCHO at Westport and surface NO$_2$ at SLAMS. On

https://doi.org/10.1021/acs.est.2c02972
Environ. Sci. Technol. 2022, 56, 15312−15327

ozone exceedance days, mean surface HCHO at Westport increased by about 3 ppb (more than 80%) averaged for the hour surrounding 1:30 PM (TROPOMI overpass) and for the aircraft sampling times during the campaign (Figure S9a). This enhancement is greater when we consider all 19 exceedance days for which TROPOMI data is available, with a 4 ppb increase in the mean (about 176%). In NYC, the regional mean surface NO_2 concentrations reported by the SLAMS during the 5-day comparison at around 1:30 PM increased from 8.4 to 10.3 ppb (+22%) and from 11.9 to 13.1 ppb (+10%) during times when airborne observations are available (Figure S9b). Regional mean concentrations of surface NO_2 around 1:30 PM increased from 9.3 to 10.8 ppb (+16%) for the 19-day comparison (Figure S9b), with enhancements observed at all individual sites in NYC (not shown).

Next, we examine changes observed by the ground-based Pandora spectrometers operating during LISTOS. The changes in NO_2-VCD_{Trop} on exceedance relative to nonexceedance days at each Pandora spectrometer site are denoted as percentages on maps to show the differences in the means (Figure 2a,b) and as box plots extending from the 25th to the 75th percentile with a horizontal line at the median and a whisker showing the range (Figure 2c). As in prior work,[85] we find that summer-averaged NO_2-VCD_{Trop} is highest at sites within or near the urban core, including Manhattan ($>1 \times 10^{16}$ molecules/cm^2), Bayonne, Queens College, and Bronx Pfizer (all $\sim 10^{16}$ molecules/cm^2), with lower summer mean NO_2-VCD_{Trop} at the shoreline sites (Westport, New Haven, Hammonasset, Outer Island, and Flax Pond; $\sim 10^{15}$ molecules/cm^2) (Figure 2c). Focusing on the TROPOMI overpass time, the average across all Pandora sites increases by 28% from the 19 nonexceedance to exceedance days. Only the upwind site to the southwest of NYC (Rutgers), shows a drop (−20%; p-value >0.01) in NO_2-VCD_{Trop} on exceedance days (Figure 2a), which agrees with surface NO_2 measurements from the co-located SLAMS monitor (−14% drop on exceedance days). The most substantial relative increase on high-ozone days occurs at Westport, CT (+107%; p-value <0.01), while a 19−49% (p-value <0.01) increase occurs at other NYC sites (Figure 2a). The larger relative enhancement in NO_2-VCD_{Trop} retrieved from the Pandora instruments versus from TROPOMI on exceedance days may reflect the more localized scale sampled by the individual spectrometers and spatial representation errors[54] in TROPOMI retrievals.

High-ozone days in NYC are accompanied by higher power plant NO_x emissions, warmer temperatures, and stronger winds (all with p-values <0.01). Figure 2d shows NO_x emissions (kg/h) from CEMS for selected exceedance days (orange) and nonexceedance days (blue) following the date classifications in Figure S2. In NYC, power plant NO_x emissions on the 5 exceedance days when the aircraft flew are 50% higher than on the five nonexceedance flight days (Figure 2d). The summed NO_x emissions for the 19 exceedance days when TROPOMI retrievals are available are 48% higher than on our selected 19 nonexceedance days. Increases in NO_2-VCD_{Trop} near NYC urban areas are possibly associated with increased energy demand on hotter high-ozone days.[91,92] High HCHO across the domain on ozone exceedance days may reflect increasing biogenic emissions from vegetation and evaporative sources[42,93−95] as regional mean temperature rises by about 5 K on exceedance days.

The top row of Figure 3 shows 10 m wind vectors, the 2 m temperatures, and the contours encompassing ∼90% of the cumulative surface influence (estimated by summing 6 h HRRR-STILT footprints outlined by trajectories initiated from 50 m above the ground) at the Westport (red) site and combined over the four NYC urban and near-urban Pandora sites (Bayonne, Manhattan, Queens College, and Bronx Pfizer in Figure S1b) (green) for the 19 exceedance versus 19 nonexceedance days. Faster winds (about +1 m/s) with a broad-scale shift in the average wind direction from southeasterly to southwesterly occur on exceedance days in NYC, suggesting a role for ozone transport from upwind regions. The HRRR-STILT footprints, however, indicate a coincident increase in local surface influence (and thus local emission sources) within NYC on exceedance days. This surface influence diagnosed with HRRR-STILT includes more transport from upwind (New Jersey) to the four NYC urban and near-urban Pandora sites (Figure S1b), as well as from Long Island Sound to Westport, CT. In contrast, on nonexceedance days, winds blow from multiple directions with a larger footprint over the ocean and to the north (top row in Figure 3). Southwesterly winds dominate in NYC during high-ozone episodes (4 of 5 days during the LISTOS campaign and 13 of 19 for the entire summer; Figure S10a), whereas wind speeds and directions are more diverse on nonexceedance days (Figure S10b).

Southwesterly winds on ozone exceedance days in NYC have been documented in previous studies focused on individual episodes as well as climatological analyses.[57,96−98] The prevailing wind patterns during high-ozone episodes in summer 2018 are similar to the dominant wind direction associated with the average summer day ozone transport along the Atlantic coast for 1991−1995, when the climatological transport to New York was from the west-southwest.[55] Consistent with the more localized influence suggested by HRRR-STILT, we find shallower planetary boundary layers on exceedance days (Text S4 and Figure S11), as noted in past studies.[22,99−102] Though stronger winds suggest additional transport of ozone and its precursors into the NYC domain from upwind sources on ozone exceedance days, we also find more local boundary layer influence, and thus presumably local sources on local ozone production, including from the higher NO_x emissions recorded in the CEMS data.

3.2. Baltimore/Washington D.C. Using only pixels over land, we find smaller increases in TROPOMI-retrieved HCHO-VCD_{Trop} (+13%; p-value <0.01) on 10 exceedance days relative to 10 nonexceedance days occurring over BAL/DC, with little rural−urban gradient (Figure S12). Regional mean NO_2-VCD_{Trop} on polluted days are higher by 5% (p-value <0.01). In contrast, NO_2-VCD_{Trop} retrieved from three suburban Pandora spectrometers is lower on ozone exceedance days by 6−22% (p-values <0.01; Figure 2b,c). There is no change (difference of around 0%) in the regional mean surface NO_2 concentrations at the SLAMS around 1:30 PM in BAL/DC (Figure S9b), but individual monitors within DC and near BAL urban centers show an increase in surface NO_2 on high-ozone days, whereas one suburban site observes a decrease (not shown).

Jin et al.[50] previously found that HCHO/NO_2-VCD_{Trop} ratios below 3.2 indicate a NO_x-saturated regime over Washington D.C., while ratios above 4.1 indicate NO_x-sensitive ozone formation, with the transitional regime falling between these values. Based on these threshold values, more than 90% pixels in BAL/DC are NO_x-sensitive as inferred from HCHO/NO_2-VCD_{Trop} ratios >4.1 on both ozone exceedance

https://doi.org/10.1021/acs.est.2c02972
Environ. Sci. Technol. 2022, 56, 15312−15327

and nonexceedance days. TROPOMI shows higher HCHO/NO_2-VCD_{Trop} ratios on ozone exceedance days (+5% on average; p-values <0.01). According to this classification, 6% more pixels (from 94 to 100%) in the domain (Figure S1c) shift into NO_x-sensitive regimes on ozone exceedance days (Table 1 and Figure S12).

High-ozone days in BAL/DC coincide with higher CEMS NO_x emissions (+68%; Figure 2d), warmer temperatures (+3 K; Figure 3), and slower surface wind speeds (about −1 m/s; Figure 3), all with p-values <0.01. Wind directions are diverse on both ozone exceedance (Figure S10c) and nonexceedance days (Figure S10d). As in NYC (Section 3.1), we find a more localized footprint of surface emission influence on ozone exceedance days in BAL/DC (bottom row of Figure 3). The meteorological situation matches the classic conceptual model of air stagnation accompanying higher temperature,[17,103−105] indicating a dominant role for local ozone production. Our findings resonate with previous studies emphasizing the impact of local industrial and traffic emissions and mesoscale meteorology (for example, boundary layer depth, humidity, air circulation) on surface ozone pollution over BAL/DC and the Chesapeake Bay.[22,106−108]

3.3. Ozone Weekend Effect. Comparing 24 Saturdays/Sundays versus 24 Tuesdays/Thursdays (Figure S3), the spatial average surface MDA8 ozone concentrations increase about +2 ppb (+4%) in NYC, with no change (∼0%) in BAL/DC. We examine TROPOMI-retrieved VCD_{Trop} of HCHO, NO_2, and HCHO/NO_2 ratios averaged over the same period over NYC (Figure S13) and BAL/DC (Figure S14), as well as in the urban cores (Table S3). The spatial average of TROPOMI-retrieved NO_2-VCD_{Trop} decreases on the weekends, with higher HCHO-VCD_{Trop} and HCHO/NO_2-VCD_{Trop} in all three urban regions of NYC, BAL, and DC (Text S2). We only find reduced NO_x emissions from power plants recorded by CEMS on weekends in the NYC and BAL urban regions (Figure S15), with cooler spatial average temperatures and weaker winds (Figure S16).

As inferred from the ratio, the ozone production regime does not change on the weekends in the urban cores of NYC and DC (Table S3). In the NYC urban center, all pixels remain NO_x-saturated as indicated by the TROPOMI-retrieved HCHO/NO_2-VCD_{Trop} ratio <2.9 (Table S3).[50] While previous analyses found a diminishing ozone weekend effect in the northeast U.S. with NO_x controls,[109,110] we still detect higher ozone and lower NO_2 concentrations and NO_x from power plant emissions on weekends. The continued existence of a weekday/weekend effect where ozone increases with lower weekend NO_x emissions implies that deeper cuts in NO_x emissions are needed to shift the ozone formation chemistry to NO_x-sensitive in the NYC urban core. By contrast, all pixels in DC urban center are always in the NO_x-sensitive regime with ratios >4.1,[50] indicating that further NO_x controls should reduce ozone, regardless of the day of week.

3.4. Uncertainties and Limitations. Earlier evaluations of version 1 TROPOMI HCHO-VCD_{Trop} and NO_2-VCD_{Trop} products showed improved performance relative to OMI, the TROPOMI predecessor instrument, with better precision (HCHO column retrieval precision improved by 25% for individual pixels[111]) and finer native spatial resolution.[112,113] However, TROPOMI-retrieved HCHO-VCD_{Trop} and NO_2-VCD_{Trop} products showed a low bias in urban regions compared with independent observations, such as GeoTASO,[61] Multiaxis differential optical absorption spectroscopy (MAX-DOAS),[111,114] and Fourier transform infrared (FTIR) measurements.[115] We assess here how these biases may influence our conclusions by applying generalized corrections based on the median biases in HCHO-VCD_{Trop} and NO_2-VCDTrop identified in previous evaluations of the same product versions. We apply these corrections at the pixel level for all days in summer 2018 (May 14−August 31) when data is available (Text S6; corrections are based on Vigouroux et al.[115] for HCHO-VCD_{Trop} and Verhoelst et al.[114] for NO_2-VCD_{Trop}). We find that the tendency toward higher HCHO-VCD_{Trop}, NO_2-VCD_{Trop}, and HCHO/NO_2 ratios on ozone exceedance days in NYC and BAL/DC does not change following this bias correction (Text S6, Table S4, and Figures S17 and S18). We emphasize, however, that the biases identified in earlier work are not universal in time and space[111,114−117] and different corrections may be more appropriate in NYC and BAL/DC.

While HCHO-VCD_{Trop}, NO_2-VCD_{Trop} and HCHO/NO_2 changes from nonexceedance to exceedance days retrieved from airborne remote sensing are consistent in sign with the TROPOMI products during the LISTOS campaign in NYC, the magnitudes differ. Compared with the GCAS/GeoTASO observations (version R1), TROPOMI retrievals (RPRO version 1) show higher absolute concentrations of HCHO-VCD_{Trop} but lower NO_2-VCD_{Trop} over NYC (Figures S4 and S5), most likely due to different sampling times and potentially reflecting differences in the retrieval products and uncertainties.[61,67,115] TROPOMI also show a smaller increase in HCHO-VCD_{Trop} on high-ozone days. The relative increase in the HCHO/NO_2-VCD_{Trop} ratio on ozone exceedance days is smaller, but TROPOMI indicates that a larger percentage of pixels within NYC shifts into transitional and NO_x-sensitive regimes (Table 1). The increase in HCHO/NO_2-VCD_{Trop} ratio on high-ozone days is smaller (from 144 to 62%) and closer to that indicated by TROPOMI (63%) when we re-grid GCAS/GeoTASO observations to the same resolution as TROPOMI, possibly because taking the spatial average across pixels (2983 to 125 pixels) reducing the variations. Findings are similar even when we apply bias corrections based on previous work to TROPOMI HCHO-VCD_{Trop} and NO_2-VCD_{Trop} (Text S6).

An inherent challenge in using the HCHO/NO_2-VCD_{Trop} ratio to study local ozone production is that the ratio may not fully describe the chemical regime because HCHO production rates can vary with NO_2.[53,54,118] Souri et al.[54] systematically evaluate and separately weight the errors associated with the retrievals, vertical column to planetary boundary layer translation, and spatial representation for daily TROPOMI (HCHO product version 2.02.01 and NO_2 version 2.2.0) in summer 2021 over the U.S. They conclude that uncertainty in the retrievals is the largest contributor to total error in HCHO/NO_2-VCD_{Trop}, with HCHO-VCD_{Trop} retrievals generally contributing larger errors than NO_2 as a result of narrower molecular absorption in the ultraviolet−visible range.[119] TROPOMI HCHO-VCD_{Trop} retrievals contain larger uncertainties than NO_2-VCD_{Trop}, which enlarge the uncertainties in using HCHO/NO_2-VCD_{Trop} ratio (Text S6 and Figures S17 and S18). Nonuniform vertical mixing in the lower troposphere also impairs the relevance of column densities for indicating surface ozone chemistry.[49,52] In addition, the relationship between column HCHO to the surface total organic reactivity, determined by the local mix of VOCs, is uncertain.[50,120]

https://doi.org/10.1021/acs.est.2c02972
Environ. Sci. Technol. 2022, 56, 15312−15327

4. DISCUSSION

The various datasets we analyzed all point toward increased HCHO and NO_2 concentrations on ozone exceedance days. We infer that these increases may reflect common drivers, such as warmer temperatures that could enhance HCHO concentrations from biogenic VOC emissions[121,122] and higher NO_x emissions from EGUs to meet rising energy demand.[91,92] Higher NO_x levels on ozone exceedance days may also enhance HCHO concentrations by facilitating VOC oxidation in a warmer environment. A source appointment study is needed to quantify the dominant emissions contributing to the observed enhancements more precisely. The increase in HCHO-VCD_{Trop} is larger than NO_2-VCD_{Trop}, leading to an overall increase in the HCHO/NO_2-VCD_{Trop} on ozone exceedance days, regardless of the city-specific initial ratio values, even in the NYC, BAL, and DC urban core areas. These findings imply a transition toward a more NO_x-sensitive photochemical environment on high-ozone days even as more NO_x is available for ozone production in NYC and BAL/DC, suggesting that additional NO_x emission reductions may effectively reduce ozone levels, especially on the most polluted days. Improvement in the products retrieved from satellite instruments and better uncertainty quantification would increase the confidence in using the VCD_{Trop} of HCHO and NO_2 as well as the HCHO/NO_2 ratio in a more quantitative manner for decision making.

Based on HCHO/NO_2-VCD_{Trop} retrieved from GCAS/GeoTASO and TROPOMI and threshold values calculated in Jin et al.,[50] the NYC urban region falls in the NO_x-saturated regime, whereas the BAL/DC region with lower summertime mean NO_2 VCD_{Trop} is more sensitive to NO_x. Earlier work also concludes that the NYC urban core remains NO_x-saturated despite a general trend across the United States, including areas in the broader NYC metropolitan region, shifting urban chemistry toward NO_x-sensitive in the past two decades.[50,51,123−125] The BAL/DC region has also been identified as becoming dominated by the NO_x-sensitive regime since the early 2000s.[108] In any urban region that remains NO_x-saturated, even though VOC emission reductions may help abate ozone locally, it would first be critical to determine whether local anthropogenic (for example, VOC from volatile chemical products[126−129]) versus biogenic emissions dominate the VOC reactivity contributing to ozone formation, especially as biogenic VOC emissions are generally not controllable. In all cases, however, reducing NO_x emissions will reduce the overall regional ozone production, and shift the urban core to NO_x-sensitive with sufficient reductions.

This study focused on the local chemistry on high versus low-ozone days in the afternoons with TROPOMI retrievals and airborne flights two to four times on a limited number of days during field campaigns in summer 2018. Ozone precursor emissions, concentrations, and photochemistry also vary diurnally. Observing diurnal variations could improve our understanding of the interactions and feedback between emissions and meteorology that shape ozone pollution distributions, including on the highest ozone days. Continuous surface HCHO concentrations measurements from more locations, such as New York Botanical Garden and Flax Pond with continuously running Picarro instruments starting fall 2021[130] may provide new insights into the diurnal variations in HCHO at the surface versus the remotely sensed column and their links to specific VOC sources. Future field campaigns, such as the Greater New York Oxidant Trace gas Halogen and Aerosol Airborne Mission (GOTHAAM; planned for summer 2023), and new anticipated satellites, such as the Tropospheric Emissions Monitoring of Pollution (TEMPO; scheduled to launch in 2023), will provide new opportunities to test the utility of applying the VCD_{Trop} of HCHO and NO_2 to infer local photochemical conditions for ozone formation.

■ ASSOCIATED CONTENT

Supporting Information

The Supporting Information is available free of charge at https://pubs.acs.org/doi/10.1021/acs.est.2c02972.

Observations using OMI retrievals (Section S1); ozone weekend effect in NYC, BAL, and DC urban centers (Section S2); calculations of NO_2-VCD_{Trop} from the Pandora spectrometers (Section S3); supplementary analysis in meteorology and transport on ozone exceedance/nonexceedance days (Section S4); sensitivity test of observed exceedance/nonexceedance differences to the selection of days (Section S5); evaluate bias and uncertainties in TROPOMI products (Section S6); data information summary (Table S1); flight sampling times (Table S2); change on weekends relative to weekdays for smaller urban core regions (Table S3); change on ozone exceedance days relative to non-exceedance days based on TROPOMI data with bias correction (Table S4); locations of surface AQS SLAMS, Pandora spectrometers, and CEMS power plants (Figure S1); days selected for high-ozone events analysis during May−August 2018 (Figure S2); days selected for ozone weekday/weekend effect analysis during May−August 2018 (Figure S3); Figure 1 for HCHO-VCD_{Trop} (Figure S4); Figure 1 for NO_2-VCD_{Trop} (Figure S5); VCD_{Trop} of HCHO, NO_2, and HCHO/NO_2 ratio from TROPOMI on ozone exceedance versus nonexceedance days during summer in NYC (Figure S6); distribution of changes in the differences in VCD_{Trop} of HCHO, NO_2, and HCHO/NO_2 ratio from randomly sampled 5-day pairs of ozone exceedance versus nonexceedance days (Figure S7); Figure S6 from OMI retrievals in NYC (Figure S8); distribution of surface HCHO at Westport and surface NO_2 at AQS SLAMS on ozone exceedance and nonexceedance days (Figure S9); daily wind patterns on days selected for high-ozone episode analysis (Figure S10); differences in the planetary boundary layer height between ozone exceedance and nonexceedance days (Figure S11); Figure S6 from TROPOMI retrievals in BAL/DC (Figure S12); VCD_{Trop} of HCHO, NO_2, and HCHO/NO_2 ratio from TROPOMI on weekends versus weekdays during summer in NYC (Figure S13); Figure S13 in BAL/DC (Figure S14); Figure 2d for weekends versus weekdays (Figure S15); temperature and wind conditions on weekends versus weekdays (Figure S16); uncertainties in TROPOMI-retrieved VCD_{Trop} of HCHO and NO_2, and HCHO/NO_2 ratio (Figure S17); and uncertainties in concentrations and ratio in percentage as divided by their absolute values (Figure S18) (PDF)

https://doi.org/10.1021/acs.est.2c02972
Environ. Sci. Technol. 2022, 56, 15312−15327

AUTHOR INFORMATION

Corresponding Author

Madankui Tao − *Lamont-Doherty Earth Observatory, Columbia University, Palisades, New York 10964, United States; Department of Earth and Environmental Sciences, Columbia University, New York, New York 10027, United States;* orcid.org/0000-0003-1255-4695; Email: mtao@ldeo.columbia.edu

Authors

Arlene M. Fiore − *Lamont-Doherty Earth Observatory, Columbia University, Palisades, New York 10964, United States; Department of Earth and Environmental Sciences, Columbia University, New York, New York 10027, United States;* Present Address: Department of Earth, Atmospheric and Planetary Sciences, Massachusetts Institute of Technology, Cambridge, Massachusetts 02139, United States

Xiaomeng Jin − *Department of Chemistry, University of California, Berkeley, Berkeley, California 94720, United States;* orcid.org/0000-0002-6895-8464

Luke D. Schiferl − *Lamont-Doherty Earth Observatory, Columbia University, Palisades, New York 10964, United States;* orcid.org/0000-0002-5047-2490

Róisín Commane − *Lamont-Doherty Earth Observatory, Columbia University, Palisades, New York 10964, United States; Department of Earth and Environmental Sciences, Columbia University, New York, New York 10027, United States;* orcid.org/0000-0003-1373-1550

Laura M. Judd − *NASA Langley Research Center, Hampton, Virginia 23681, United States*

Scott Janz − *NASA Goddard Space Flight Center, Greenbelt, Maryland 20771, United States*

John T. Sullivan − *NASA Goddard Space Flight Center, Greenbelt, Maryland 20771, United States*

Paul J. Miller − *Northeast States for Coordinated Air Use Management, Boston, Massachusetts 02111, United States*

Alexandra Karambelas − *Northeast States for Coordinated Air Use Management, Boston, Massachusetts 02111, United States;* orcid.org/0000-0003-1886-7000

Sharon Davis − *New Jersey Department of Environmental Protection, Trenton, New Jersey 08625, United States*

Maria Tzortziou − *The City College of New York, New York, New York 10031, United States*

Lukas Valin − *US Environmental Protection Agency, Research Triangle Park, North Carolina 27711, United States*

Andrew Whitehill − *US Environmental Protection Agency, Research Triangle Park, North Carolina 27711, United States*

Kevin Civerolo − *New York State Department of Environmental Conservation, Albany, New York 12233, United States*

Yuhong Tian − *New York State Department of Environmental Conservation, Albany, New York 12233, United States*

Complete contact information is available at: https://pubs.acs.org/10.1021/acs.est.2c02972

Author Contributions

All authors have given approval to the final version of the manuscript.

Notes

The authors declare no competing financial interest.

NYSERDA has not reviewed the information contained herein, and the opinions expressed in this article do not necessarily reflect those of NYSERDA or the State of New York. The views expressed in this article are those of the authors and do not necessarily represent the views or the policies of the U.S. Environmental Protection Agency.

ACKNOWLEDGMENTS

This work was supported by NASA Health & Air Quality Applied Sciences Team (NNX16AQ20G and 80NSSC21K0509). L.D.S. and R.C. were supported by the NOAA Climate Program Office's Atmospheric Chemistry, Carbon Cycle, and Climate program (grant nos. NA20OAR4310306 and NA21OAR4310235). Support for A.K. and P.J.M. was provided by New York State Energy Research and Development Authority (NYSERDA) Agreement No. 101132. Additional support for OWLETS-2 campaign observations was provided by NASA Tropospheric Composition Program and the Maryland Department of the Environment (MDE).

REFERENCES

(1) Karakatsani, A.; Samoli, E.; Rodopoulou, S.; Dimakopoulou, K.; Papakosta, D.; Spyratos, D.; Grivas, G.; Tasi, S.; Angelis, N.; Thirios, A.; Tsiotsios, A.; Katsouyanni, K. Weekly Personal Ozone Exposure and Respiratory Health in a Panel of Greek Schoolchildren. *Environ. Health Perspect.* **2017**, *125*, No. 077017.

(2) Jerrett, M.; Burnett, R. T.; Beckerman, B. S.; Turner, M. C.; Krewski, D.; Thurston, G.; Martin, R. V.; Van Donkelaar, A.; Hughes, E.; Shi, Y.; Gapstur, S. M.; Thun, M. J.; Pope, C. A. Spatial Analysis of Air Pollution and Mortality in California. *Am. J. Respir. Crit. Care Med.* **2013**, *188*, 593−599.

(3) Dedoussi, I. C.; Eastham, S. D.; Monier, E.; Barrett, S. R. H. Premature Mortality Related to United States Cross-State Air Pollution. *Nature* **2020**, *578*, 261−265.

(4) Fuhrer, J.; Val Martin, M.; Mills, G.; Heald, C. L.; Harmens, H.; Hayes, F.; Sharps, K.; Bender, J.; Ashmore, M. R. Current and Future Ozone Risks to Global Terrestrial Biodiversity and Ecosystem Processes. *Ecol. Evol.* **2016**, *6*, 8785−8799.

(5) Avnery, S.; Mauzerall, D. L.; Liu, J.; Horowitz, L. W. Global Crop Yield Reductions Due to Surface Ozone Exposure: 1. Year 2000 Crop Production Losses and Economic Damage. *Atmos. Environ.* **2011**, *45*, 2284−2296.

(6) U.S. Environmental Protection Agency. National Ambient Air Quality Standards for Ozone. *Fed. Regist.* **2015**, *80*, 65291−65468.

(7) Karambelas, A.*LISTOS: Toward a Better Understanding of New York City's Ozone Pollution Problem*. https://www.nescaum.org/documents/listos-toward-a-better-understanding-of-new-york-city2019s-ozone-pollution-problem (accessed Sept 6, 2022).

(8) Sullivan, J. T.; Berkoff, T.; Gronoff, G.; Knepp, T.; Pippin, M.; Allen, D.; Twigg, L.; Swap, R.; Tzortziou, M.; Thompson, A. M.; Stauffer, R. M.; Wolfe, G. M.; Flynn, J.; Pusede, S. E.; Judd, L. M.; Moore, W.; Baker, B. D.; Al-Saadi, J.; Mcgee, T. J. The Ozone Water-Land Environmental Transition Study: An Innovative Strategy for Understanding Chesapeake Bay Pollution Events. *Bull. Am. Meteorol. Soc.* **2019**, *100*, 291−306.

(9) U.S. Environmental Protection Agency. *Green Book 8-Hour Ozone*, 2015. https://www.epa.gov/green-book/green-book-8-hour-ozone-2015-area-information (accessed March 3, 2022).

(10) Blanchard, C. L.; Shaw, S. L.; Edgerton, E. S.; Schwab, J. J. Emission Influences on Air Pollutant Concentrations in New York State: I. Ozone. *Atmos. Environ. X* **2019**, *3*, No. 100033.

(11) Masiol, M.; Hopke, P. K.; Felton, H. D.; Frank, B. P.; Rattigan, O. V.; Wurth, M. J.; LaDuke, G. H. Analysis of Major Air Pollutants and Submicron Particles in New York City and Long Island. *Atmos. Environ.* **2017**, *148*, 203−214.

(12) Trainer, M.; Williams, E. J.; Parrish, D. D.; Buhr, M. P.; Allwine, E. J.; Westberg, H. H.; Fehsenfeld, F. C.; Liu, S. C. Models and Observations of the Impact of Natural Hydrocarbons on Rural Ozone. *Nature* **1987**, *329*, 705−707.
(13) Pun, B. K.; Wu, S.-Y.; Seigneur, C. Contribution of Biogenic Emissions to the Formation of Ozone and Particulate Matter in the Eastern United States. *Environ. Sci. Technol.* **2002**, *36*, 3586−3596.
(14) Jaffe, D. A.; O'Neill, S. M.; Larkin, N. K.; Holder, A. L.; Peterson, D. L.; Halofsky, J. E.; Rappold, A. G. Wildfire and Prescribed Burning Impacts on Air Quality in the United States. *J. Air Waste Manage. Assoc.* **2020**, *70*, 583−615.
(15) DeBell, L. J.; Talbot, R. W.; Dibb, J. E.; Munger, J. W.; Fischer, E. V.; Frolking, S. E. A Major Regional Air Pollution Event in the Northeastern United States Caused by Extensive Forest Fires in Quebec, Canada. *J. Geophys. Res.: Atmos.* **2004**, *109*, No. D19305.
(16) Colarco, P. R.; Schoeberl, M. R.; Doddridge, B. G.; Marufu, L. T.; Torres, O.; Welton, E. J. Transport of Smoke from Canadian Forest Fires to the Surface near Washington, D.C.: Injection Height, Entrainment, and Optical Properties. *J. Geophys. Res.: Atmos.* **2004**, *109*, No. D06203.
(17) Porter, W. C.; Heald, C. L. The Mechanisms and Meteorological Drivers of the Summertime Ozone-Temperature Relationship. *Atmos. Chem. Phys.* **2019**, *19*, 13367−13381.
(18) Zhao, K.; Bao, Y.; Huang, J.; Wu, Y.; Moshary, F.; Arend, M.; Wang, Y.; Lee, X. A High-Resolution Modeling Study of a Heat Wave-Driven Ozone Exceedance Event in New York City and Surrounding Regions. *Atmos. Environ.* **2019**, *199*, 368−379.
(19) Rubino, R. A.; Bruckman, L.; Magyar, J. Ozone Transport. *J. Air Pollut. Control Assoc.* **1976**, *26*, 972−975.
(20) Zhang, J.; Mak, J.; Wei, Z.; Cao, C.; Ninneman, M.; Marto, J.; Schwab, J. J. Long Island Enhanced Aerosol Event during 2018 LISTOS: Association with Heatwave and Marine Influences. *Environ. Pollut.* **2021**, *270*, No. 116299.
(21) Dreessen, J.; Orozco, D.; Boyle, J.; Szymborski, J.; Lee, P.; Flores, A.; Sakai, R. K. Observed Ozone Over the Chesapeake Bay Land-Water Interface: The Hart-Miller Island Pilot Project. *J. Air Waste Manage. Assoc.* **2019**, *69*, 1312−1330.
(22) Goldberg, D. L.; Loughner, C. P.; Tzortziou, M.; Stehr, J. W.; Pickering, K. E.; Marufu, L. T.; Dickerson, R. R. Higher Surface Ozone Concentrations over the Chesapeake Bay than over the Adjacent Land: Observations and Models from the DISCOVER-AQ and CBODAQ Campaigns. *Atmos. Environ.* **2014**, *84*, 9−19.
(23) Loughner, C. P.; Tzortziou, M.; Follette-Cook, M.; Pickering, K. E.; Goldberg, D.; Satam, C.; Weinheimer, A.; Crawford, J. H.; Knapp, D. J.; Montzka, D. D.; Diskin, G. S.; Dickerson, R. R. Impact of Bay-Breeze Circulations on Surface Air Quality and Boundary Layer Export. *J. Appl. Meteorol. Climatol.* **2014**, *53*, 1697−1713.
(24) U. S. Census Bureau. *Change in Resident Population of the 50 States, the District of Columbia, and Puerto Rico: 1910 to 2020*https://www2.census.gov/programs-surveys/decennial/2020/data/apportionment/population-change-data-table.pdf (accessed March 25, 2022).
(25) Sillman, S. The Relation Between Ozone, NO_x, and Hydrocarobons in Urban and Polluted Rural Environments. *Atmos. Environ.* **1999**, *33*, 1821−1845.
(26) Reimann, S.; Lewis, A. C.Anthropogenic VOCs. In *Volatile Organic Compounds in the Atmosphere*; John Wiley & Sons, Ltd., 2007; pp 33−81.
(27) Chen, X.; Millet, D. B.; Singh, H. B.; Wisthaler, A.; Apel, E. C.; Atlas, E. L.; Blake, D. R.; Bourgeois, I.; Brown, S. S.; Crounse, J. D.; de Gouw, J. A.; Flocke, F. M.; Fried, A.; Heikes, B. G.; Hornbrook, R. S.; Mikoviny, T.; Min, K.-E.; Müller, M.; Neuman, J. A.; O'Sullivan, D. W.; Peischl, J.; Pfister, G. G.; Richter, D.; Roberts, J. M.; Ryerson, T. B.; Shertz, S. R.; Thompson, C. R.; Treadaway, V.; Veres, P. R.; Walega, J.; Warneke, C.; Washenfelder, R. A.; Weibring, P.; Yuan, B. On the Sources and Sinks of Atmospheric VOCs: An Integrated Analysis of Recent Aircraft Campaigns Over North America. *Atmos. Chem. Phys.* **2019**, *19*, 9097−9123.
(28) Steiner, A. H.; Goldstein, A. L.Biogenic VOCs. *Volatile Organic Compounds in the Atmosphere*; John Wiley & Sons, Ltd., 2007; pp 82−128.
(29) Toro, C.; Foley, K.; Simon, H.; Henderson, B.; Baker, K. R.; Eyth, A.; Timin, B.; Appel, W.; Luecken, D.; Beardsley, M.; Sonntag, D.; Possiel, N.; Roberts, S. Evaluation of 15 Years of Modeled Atmospheric Oxidized Nitrogen Compounds across the Contiguous United States. *Elementa* **2021**, *9*, No. 00158.
(30) Kleinman, L. I. Low and High NO_x Tropospheric Photochemistry. *J. Geophys. Res.* **1994**, *99*, 16831−16838.
(31) Kleinman, L. I. The Dependence of Tropospheric Ozone Production Rate on Ozone Precursors. *Atmos. Environ.* **2005**, *39*, 575−586.
(32) Sillman, S.Tropospheric Ozone and Photochemical Smog. *Treatise on Geochemistry*; Elsevier: Amsterdam, 2003; pp 407−431.
(33) Tonnesen, G. S.; Dennis, R. L. Analysis of Radical Propagation Efficiency to Assess Ozone Sensitivity to Hydrocarbons and NO_x 1. Local Indicators of Instantaneous Odd Oxygen Production Sensitivity. *J. Geophys. Res.: Atmos.* **2000**, *105*, 9213−9225.
(34) Sillman, S.Overview: Tropospheric Ozone, Smog and Ozone-NO_x-VOC Sensitivity. http://www-personal.umich.edu/~sillman/ (accessed Feb 4, 2022).
(35) Kleinman, L. I.; Daum, P. H.; Lee, J. H.; Lee, Y.-N.; Nunnermacker, L. J.; Springston, S. R.; Newman, L.; Weinstein-Lloyd, J.; Sillman, S. Dependence of Ozone Production on NO and Hydrocarbons in the Troposphere. *Geophys. Res. Lett.* **1997**, *24*, 2299−2302.
(36) Sillman, S.; Logan, J. A.; Wofsy, S. C. The Sensitivity of Ozone to Nitrogen Oxides and Hydrocarbons in Regional Ozone Episodes. *J. Geophys. Res.: Atmos.* **1990**, *95*, 1837−1851.
(37) Martin, R. V.; Fiore, A. M.; Van Donkelaar, A. Space-Based Diagnosis of Surface Ozone Sensitivity to Anthropogenic Emissions. *Geophys. Res. Lett.* **2004**, *31*, No. L06120.
(38) Duncan, B. N.; Yoshida, Y.; Olson, J. R.; Sillman, S.; Martin, R. V.; Lamsal, L.; Hu, Y.; Pickering, K. E.; Retscher, C.; Allen, D. J.; Crawford, J. H. Application of OMI Observations to a Space-Based Indicator of NO_x and VOC Controls on Surface Ozone Formation. *Atmos. Environ.* **2010**, *44*, 2213−2223.
(39) Li, D.; Wang, S.; Xue, R.; Zhu, J.; Zhang, S.; Sun, Z.; Zhou, B. OMI-Observed HCHO in Shanghai, China, During 2010-2019 and Ozone Sensitivity Inferred by an Improved HCHO/NO_2 Ratio. *Atmos. Chem. Phys.* **2021**, *21*, 15447−15460.
(40) Jin, X.; Holloway, T. Spatial and Temporal Variability of Ozone Sensitivity over China Observed from the Ozone Monitoring Instrument. *J. Geophys. Res.: Atmos.* **2015**, *120*, 7229−7246.
(41) Palmer, P. I.; Jacob, D. J.; Chance, K.; Martin, R. V.; Spurr, R. J. D.; Kurosu, T. P.; Bey, I.; Yantosca, R.; Fiore, A.; Li, Q. Air Mass Factor Formulation for Spectroscopic Measurements From Satellites: Application to Formaldehyde Retrievals From the Global Ozone Monitoring Experiment. *J. Geophys. Res.: Atmos.* **2001**, *106*, 14539−14550.
(42) Palmer, P. I.; Jacob, D. J.; Fiore, A. M.; Martin, R. V.; Chance, K.; Kurosu, T. P. Mapping Isoprene Emissions Over North America Using Formaldehyde Column Observations From Space. *J. Geophys. Res.: Atmos.* **2003**, *108*, No. 4180.
(43) Zhu, L.; Jacob, D. J.; Mickley, L. J.; Marais, E. A.; Cohan, D. S.; Yoshida, Y.; Duncan, B. N.; González Abad, G.; Chance, K. V. Anthropogenic Emissions of Highly Reactive Volatile Organic Compounds in Eastern Texas Inferred From Oversampling of Satellite (OMI) Measurements of HCHO Columns. *Environ. Res. Lett.* **2014**, *9*, No. 114004.
(44) Hong, Q.; Liu, C.; Hu, Q.; Zhang, Y.; Xing, C.; Su, W.; Ji, X.; Xiao, S. Evaluating the Feasibility of Formaldehyde Derived from Hyperspectral Remote Sensing as a Proxy for Volatile Organic Compounds. *Atmos. Res.* **2021**, *264*, No. 105777.
(45) Valin, L. C.; Fiore, A. M.; Chance, K.; González Abad, G. The Role of OH Production in Interpreting the Variability of CH_2O Columns in the Southeast U.S. *J. Geophys. Res.: Atmos.* **2016**, *121*, 478−493.

(46) Travis, K. R.; Judd, L. M.; Crawford, J. H.; Chen, G.; Szykman, J.; Whitehill, A.; Valin, L. C.; Spinei, E.; Janz, S.; Nowlan, C. R.; Kwon, H.-A.; Fried, A.; Walega, J. Can Column Formaldehyde Observations Inform Air Quality Monitoring Strategies for Ozone and Related Photochemical Oxidants? *J. Geophys. Res.: Atmos.* **2022**, *127*, No. e2022JD036638.
(47) Schroeder, J. R.; Crawford, J. H.; Fried, A.; Walega, J.; Weinheimer, A.; Wisthaler, A.; Müller, M.; Mikoviny, T.; Chen, G.; Shook, M.; Blake, D. R.; Diskin, G.; Estes, M.; Thompson, A. M.; Lefer, B. L.; Long, R.; Mattson, E. Formaldehyde Column Density Measurements as a Suitable Pathway to Estimate Near-Surface Ozone Tendencies from Space. *J. Geophys. Res.: Atmos.* **2016**, *121*, 13088.
(48) Choi, Y.; Souri, A. H. Chemical Condition and Surface Ozone in Large Cities of Texas During the Last Decade: Observational Evidence From OMI, CAMS, and Model Analysis. *Remote Sens. Environ.* **2015**, *168*, 90−101.
(49) Jin, X.; Fiore, A. M.; Murray, L. T.; Valin, L. C.; Lamsal, L. N.; Duncan, B.; Folkert Boersma, K.; De Smedt, I.; Abad, G. G.; Chance, K.; Tonnesen, G. S. Evaluating a Space-Based Indicator of Surface Ozone-NO_x-VOC Sensitivity Over Midlatitude Source Regions and Application to Decadal Trends. *J. Geophys. Res.: Atmos.* **2017**, *122*, 10439−10461.
(50) Jin, X.; Fiore, A.; Boersma, K. F.; De Smedt, I.; Valin, L. Inferring Changes in Summertime Surface Ozone-NO_x-VOC Chemistry Over U.S. Urban Areas From Two Decades of Satellite and Ground-Based Observations. *Environ. Sci. Technol.* **2020**, *54*, 6518−6529.
(51) Koplitz, S.; Simon, H.; Henderson, B.; Liljegren, J.; Tonnesen, G.; Whitehill, A.; Wells, B. Changes in Ozone Chemical Sensitivity in the United States from 2007 to 2016. *ACS Environ. Au* **2022**, *2*, 206.
(52) Schroeder, J. R.; Crawford, J. H.; Fried, A.; Walega, J.; Weinheimer, A.; Wisthaler, A.; Müller, M.; Mikoviny, T.; Chen, G.; Shook, M.; Blake, D. R.; Tonnesen, G. S. New Insights into the Column CH_2O/NO_2 Ratio as an Indicator of near-Surface Ozone Sensitivity. *J. Geophys. Res.: Atmos.* **2017**, *122*, 8885−8907.
(53) Souri, A. H.; Nowlan, C. R.; Wolfe, G. M.; Lamsal, L. N.; Janz, S. J.; Fried, A.; Chan, C. E.; Gonz, G.; Blake, D. R.; Weinheimer, A. J.; Diskin, G. S.; Liu, X.; Chance, K. Revisiting the Effectiveness of $HCHO/NO_2$ Ratios for Inferring Ozone Sensitivity to Its Precursors Using High Resolution Airborne Remote Sensing Observations in a High Ozone Episode During the KORUS-AQ Campaign. *Atmos. Environ.* **2020**, *224*, No. 117341.
(54) Souri, A. H.; Johnson, M. S.; Wolfe, G. M.; Crawford, J. H.; Fried, A.; Wisthaler, A.; Brune, W. H.; Blake, D. R.; Weinheimer, A. J.; Verhoelst, T.; Compernolle, S.; Pinardi, G.; Vigouroux, C.; Langerock, B.; Choi, S.; Lamsal, L.; Zhu, L.; Sun, S.; Cohen, R. C.; Min, K.-E.; Cho, C.; Philip, S.; Liu, X.; Chance, K. Characterization of Errors in Satellite-Based $HCHO/NO_2$ Tropospheric Column Ratios with Respect to Chemistry, Column to PBL Translation, Spatial Representation, and Retrieval Uncertainties. *Atmos. Chem. Phys. Discuss.* **2022**, *2022*, 1−43.
(55) Schichtel, B. A.; Husar, R. B. Eastern North American Transport Climatology during High- and Low-Ozone Days. *Atmos. Environ.* **2001**, *35*, 1029−1038.
(56) St John, J. C.; Chameides, W. L. Climatology of Ozone Exceedences in the Atlanta Metropolitan Area: 1-Hour vs 8-Hour Standard and the Role of Plume Recirculation Air Pollution Episodes. *Environ. Sci. Technol.* **1997**, *31*, 2797−2804.
(57) Brankov, E.; Rao, S. T.; Porter, P. S. A Trajectory-Clustering-Correlation Methodology for Examining the Long-Range Transport of Air Pollutants. *Atmos. Environ.* **1998**, *32*, 1525−1534.
(58) Eder, B. K.; Davis, J. M.; Bloomfield, P. A Characterization of the Spatiotemporal Variability of Non-Urban Ozone Concentrations over the Eastern United States. *Atmos. Environ., Part A* **1993**, *27*, 2645−2668.
(59) Wilcoxon, F. Individual Comparisons by Ranking Methods. *Biom. Bull.* **1945**, *1*, 80−83.
(60) Pratt, J. W. Remarks on Zeros and Ties in the Wilcoxon Signed Rank Procedures. *J. Am. Stat. Assoc.* **1959**, *54*, 655−667.
(61) Judd, L. M.; Al-Saadi, J. A.; Szykman, J. J.; Valin, L. C.; Janz, S. J.; Kowalewski, M. G.; Eskes, H. J.; Pepijn Veefkind, J.; Cede, A.; Mueller, M.; Gebetsberger, M.; Swap, R.; Bradley Pierce, R.; Nowlan, C. R.; González Abad, G.; Nehrir, A.; Williams, D. Evaluating Sentinel-5p TROPOMI Tropospheric NO_2 Column Densities With Airborne and Pandora Spectrometers Near New York City and Long Island Sound. *Atmos. Meas. Tech.* **2020**, *13*, 6113−6140.
(62) Kowalewski, M. G.; Janz, S. J. In *Remote Sensing Capabilities of the GEO-CAPE Airborne Simulator*, Proceedings of Earth Observing Systems XIX, 2014, 92181I.
(63) Nowlan, C. R.; Liu, X.; Janz, S. J.; Kowalewski, M. G.; Chance, K.; Follette-Cook, M. B.; Fried, A.; González Abad, G.; Herman, J. R.; Judd, L. M.; Kwon, H.-A.; Loughner, C. P.; Pickering, K. E.; Richter, D.; Spinei, E.; Walega, J.; Weibring, P.; Weinheimer, A. J. Nitrogen Dioxide and Formaldehyde Measurements from the GEOstationary Coastal and Air Pollution Events (GEO-CAPE) Airborne Simulator over Houston, Texas. *Atmos. Meas. Tech.* **2018**, *11*, 5941−5964.
(64) Leitch, J. W.; Delker, T.; Good, W.; Ruppert, L.; Murcray, F.; Chance, K.; Liu, X.; Nowlan, C.; Janz, S. J.; Krotkov, N. A.; Pickering, K. E.; Kowalewski, M.; Wang, J. In *The GeoTASO Airborne Spectrometer Project*, Proc. SPIE 9218, Earth Observing Systems XIX, 2014, 92181H.
(65) Nowlan, C. R.; Liu, X.; Leitch, J. W.; Chance, K.; González Abad, G.; Liu, C.; Zoogman, P.; Cole, J.; Delker, T.; Good, W.; Murcray, F.; Ruppert, L.; Soo, D.; Follette-Cook, M. B.; Janz, S. J.; Kowalewski, M. G.; Loughner, C. P.; Pickering, K. E.; Herman, J. R.; Beaver, M. R.; Long, R. W.; Szykman, J. J.; Judd, L. M.; Kelley, P.; Luke, W. T.; Ren, X.; Al-Saadi, J. A. Nitrogen Dioxide Observations From the Geostationary Trace Gas and Aerosol Sensor Optimization (GeoTASO) Airborne Instrument: Retrieval Algorithm and Measurements During DISCOVER-AQ Texas 2013. *Atmos. Meas. Tech.* **2016**, *9*, 2647−2668.
(66) Judd, L. M.; Al-Saadi, J. A.; Janz, S. J.; Kowalewski, M. J. G.; Bradley Pierce, R.; Szykman, J. J.; Valin, L. C.; Swap, R.; Cede, A.; Mueller, M.; Tiefengraber, M.; Abuhassan, N.; Williams, D. Evaluating the Impact of Spatial Resolution on Tropospheric NO_2 Column Comparisons Within Urban Areas Using High-Resolution Airborne Data. *Atmos. Meas. Tech.* **2019**, *12*, 6091−6111.
(67) Nowlan, C. R.; Liu, X.; Janz, S. J.; Kowalewski, M. G.; Chance, K.; Follette-Cook, M. B.; Fried, A.; González Abad, G.; Herman, J. R.; Judd, L. M.; Kwon, H. A.; Loughner, C. P.; Pickering, K. E.; Richter, D.; Spinei, E.; Walega, J.; Weibring, P.; Weinheimer, A. J. Nitrogen Dioxide and Formaldehyde Measurements from the GEOstationary Coastal and Air Pollution Events (GEO-CAPE) Airborne Simulator over Houston, Texas. *Atmos. Meas. Tech.* **2018**, *11*, 5941−5964.
(68) Lamsal, L. N.; Janz, S. J.; Krotkov, N. A.; Pickering, K. E.; Spurr, R. J. D.; Kowalewski, M. G.; Loughner, C. P.; Crawford, J. H.; Swartz, W. H.; Herman, J. R. High-Resolution NO_2 Observations from the Airborne Compact Atmospheric Mapper: Retrieval and Validation. *J. Geophys. Res.: Atmos.* **2017**, *122*, 1953−1970.
(69) Veefkind, J. P.; Aben, I.; McMullan, K.; Förster, H.; de Vries, J.; Otter, G.; Claas, J.; Eskes, H. J.; de Haan, J. F.; Kleipool, Q.; van Weele, M.; Hasekamp, O.; Hoogeveen, R.; Landgraf, J.; Snel, R.; Tol, P.; Ingmann, P.; Voors, R.; Kruizinga, B.; Vink, R.; Visser, H.; Levelt, P. F. TROPOMI on the ESA Sentinel-5 Precursor: A GMES Mission for Global Observations of the Atmospheric Composition for Climate, Air Quality and Ozone Layer Applications. *Remote Sens. Environ.* **2012**, *120*, 70−83.
(70) Copernicus Sentinel data processed by ESA, G. A. C. (DLR). *Sentinel-5P TROPOMI Tropospheric Formaldehyde HCHO 1-Orbit L2 7km x 3.5km*; Goddard Earth Sciences Data and Information Services Center (GES DISC): Greenbelt, MD, 2019. DOI: 10.5270/S5P-tjlxfd2.
(71) Koninklijk Nederlands Meteorologisch Instituut (KNMI). *Sentinel-5P TROPOMI Tropospheric NO_2 1-Orbit L2 7km x 3.5km*; Goddard Earth Sciences Data and Information Services Center (GES DISC): Greenbelt, MD, 2018. DOI: 10.5270/S5P-s4ljg54.
(72) Eskes, H. J.; Eichmann, K.-U.S5P Mission Performance Centre Nitrogen Dioxide [L2__NO2___] Readme. https://sentinel.esa.int/

documents/247904/3541451/Sentinel-5P-Nitrogen-Dioxide-Level-2-Product-Readme-File (accessed Aug 16, 2022).
(73) De Smedt, I.; Romahn, F.; Eichmann, K.-U.S5P Mission Performance Centre Formaldehyde [L2__HCHO___] Readme. https://sentinels.copernicus.eu/documents/247904/3541451/Sentinel-5P-Formaldehyde-Readme.pdf (accessed Aug 16, 2022).
(74) Hastings, D. A.; Dunbar, P. K.Global Land One-kilometer Base Elevation (GLOBE) Digital Elevation Model, Documentation. https://www.ngdc.noaa.gov/mgg/topo/report/globedocumentationmanual.pdf (accessed Sept 2 , 2022).
(75) Herndon, S. C.; Zahniser, M. S.; Nelson, D. D., Jr.; Shorter, J.; McManus, J. B.; Jiménez, R.; Warneke, C.; de Gouw, J. A. Airborne Measurements of HCHO and HCOOH during the New England Air Quality Study 2004 Using a Pulsed Quantum Cascade Laser Spectrometer. *J. Geophys. Res.: Atmos.* **2007**, *112*, No. D10S03.
(76) US EPA. Quality Assurance Guidance Document 2.3. Reference Method for the Determination of Nitrogen Dioxide in the Atmosphere (Chemiluminescence). https://www3.epa.gov/ttnamti1/files/ambient/pm25/qa/no2.pdf (accessed Aug 19, 2022).
(77) Connecticut Department of Energy and Environmental Protection/Bureau of Air Management. Connecticut 2019 Annual Air Monitoring Network Plan. https://portal.ct.gov/-/media/DEEP/air_monitoring/Monitoring_Plans/CT2019NetworkPlanFinal.pdf (accessed Sep 6, 2022).
(78) New Jersey Department of Environmental Protection/Bureau of Air Monitoring. Ambient Air Monitoring Network Plan 2018. https://www.nj.gov/dep/airmon/pdf/NJ-Network-Plan-2018.pdf (accessed Sept 6, 2022).
(79) Szykman, J.; Swap, R.; Lefer, B.; Valin, L.; Lee, S. C.; Fioletov, V.; Zhao, X.; Davies, J.; Williams, D.; Abuhassan, N.; Shalaby, L.; Cede, A.; Tiefengraber, M.; Mueller, M.; Kotsakis, A.; Santos, F.; Robinson, J.Pandora: Connecting in-Situ and Satellite Monitoring in Support of the Canada − U.S. Air Quality Agreement*EM: Air Waste Manage. Assoc. Mag. Environ. Managers*, **2019**, 29−35.
(80) Tzortziou, M.; Herman, J. R.; Cede, A.; Abuhassan, N. High Precision, Absolute Total Column Ozone Measurements From the Pandora Spectrometer System: Comparisons With Data From a Brewer Double Monochromator and Aura OMI. *J. Geophys. Res.: Atmos.* **2012**, *117*, No. D16303.
(81) Herman, J.; Cede, A.; Spinei, E.; Mount, G.; Tzortziou, M.; Abuhassan, N. NO_2 Column Amounts From Ground-Based Pandora and MFDOAS Spectrometers Using the Direct-Sun DOAS Technique: Intercomparisons and Application to OMI Validation. *J. Geophys. Res.: Atmos.* **2009**, *114*, No. D13307.
(82) Herman, J.; Spinei, E.; Fried, A.; Kim, J.; Kim, J.; Kim, W.; Cede, A.; Abuhassan, N.; Segal-Rozenhaimer, M. NO_2 and HCHO Measurements in Korea from 2012 to 2016 from Pandora Spectrometer Instruments Compared with OMI Retrievals and with Aircraft Measurements during the KORUS-AQ Campaign. *Atmos. Meas. Tech.* **2018**, *11*, 4583−4603.
(83) Spinei, E.; Whitehill, A.; Fried, A.; Tiefengraber, M.; Knepp, T. N.; Herndon, S.; Herman, J. R.; Müller, M.; Abuhassan, N.; Cede, A.; Richter, D.; Walega, J.; Crawford, J.; Szykman, J.; Valin, L.; Williams, D. J.; Long, R.; Swap, R. J.; Lee, Y.; Nowak, N.; Poche, B. The First Evaluation of Formaldehyde Column Observations by Improved Pandora Spectrometers During The KORUS-AQ Field Study. *Atmos. Meas. Tech.* **2018**, *11*, 4943−4961.
(84) Tzortziou, M.; Parker, O.; Lamb, B.; Herman, J. R.; Lamsal, L.; Stauffer, R.; Abuhassan, N. Atmospheric Trace Gas (NO_2 and O_3) Variability in South Korean Coastal Waters, and Implications for Remote Sensing of Coastal Ocean Color Dynamics. *Remote Sens.* **2018**, *10*, No. 1587.
(85) Tzortziou, M.; Kwong, C. F.; Goldberg, D.; Schiferl, L.; Commane, R.; Abuhassan, N.; Szykman, J. J.; Valin, L. C. Declines and Peaks in NO_2 Pollution during the Multiple Waves of the COVID-19 Pandemic in the New York Metropolitan Area. *Atmos. Chem. Phys.* **2022**, *22*, 2399−2417.
(86) Spinei, E.; Tiefengraber, M.; Müller, M.; Gebetsberger, M.; Cede, A.; Valin, L.; Szykman, J.; Whitehill, A.; Kotsakis, A.; Santos, F.; Abbuhasan, N.; Zhao, X.; Fioletov, V.; Lee, S. C.; Swap, R. Effect of Polyoxymethylene (POM-H Delrin) Off-Gassing Within the Pandora Head Sensor on Direct-Sun and Multi-Axis Formaldehyde Column Measurements in 2016–2019. *Atmos. Meas. Tech.* **2021**, *14*, 647−663.
(87) Herman, J.; Abuhassan, N.; Kim, J.; Kim, J.; Dubey, M.; Raponi, M.; Tzortziou, M. Underestimation of Column \chem-{NO_{2}} Amounts from the OMI Satellite Compared to Diurnally Varying Ground-Based Retrievals from Multiple PANDORA Spectrometer Instruments. *Atmos. Meas. Tech.* **2019**, *12*, 5593−5612.
(88) U.S. Environmental Protection Agency. *Air Markets Program Data*. https://ampd.epa.gov/ampd/ (accessed Feb 4, 2022).
(89) Xia, Y.; Mitchell, K.; Ek, M.; Sheffield, J.; Cosgrove, B.; Wood, E.; Luo, L.; Alonge, C.; Wei, H.; Meng, J.; Livneh, B.; Lettenmaier, D.; Koren, V.; Duan, Q.; Mo, K.; Fan, Y.; Mocko, D. Continental-Scale Water and Energy Flux Analysis and Validation for the North American Land Data Assimilation System Project Phase 2 (NLDAS-2): 1. Intercomparison and Application of Model Products. *J. Geophys. Res.: Atmos.* **2012**, *117*, No. D03109.
(90) He, H.; Vinnikov, K. Y.; Krotkov, N. A.; Edgerton, E. S.; Schwab, J. J.; Dickerson, R. R. Chemical Climatology of Atmospheric Pollutants in the Eastern United States: Seasonal/Diurnal Cycles and Contrast Under Clear/Cloudy Conditions for Remote Sensing. *Atmos. Environ.* **2019**, *206*, 85−107.
(91) Abel, D.; Holloway, T.; Kladar, R. M.; Meier, P.; Ahl, D.; Harkey, M.; Patz, J. Response of Power Plant Emissions to Ambient Temperature in the Eastern United States. *Environ. Sci. Technol.* **2017**, *51*, 5838−5846.
(92) He, H.; Hembeck, L.; Hosley, K. M.; Canty, T. P.; Salawitch, R. J.; Dickerson, R. R. High Ozone Concentrations on Hot Days: The Role of Electric Power Demand and NO_x Emissions. *Geophys. Res. Lett.* **2013**, *40*, 5291−5294.
(93) Guenther, A. B.; Zimmerman, P. R.; Harley, P. C.; Monson, R. K.; Fall, R. Isoprene and Monoterpene Emission Rate Variability: Model Evaluations and Sensitivity Analyses. *J. Geophys. Res.: Atmos.* **1993**, *98*, 12609−12617.
(94) Mäki, M.; Heinonsalo, J.; Hellén, H.; Bäck, J. Contribution of Understorey Vegetation and Soil Processes to Boreal Forest Isoprenoid Exchange. *Biogeosciences* **2017**, *14*, 1055−1073.
(95) Debevec, C.; Sauvage, S.; Gros, V.; Sellegri, K.; Sciare, J.; Pikridas, M.; Stavroulas, I.; Leonardis, T.; Gaudion, V.; Depelchin, L.; Fronval, I.; Sarda-Esteve, R.; Baisnée, D.; Bonsang, B.; Savvides, C.; Vrekoussis, M.; Locoge, N. Driving Parameters of Biogenic Volatile Organic Compounds and Consequences on New Particle Formation Observed at an Eastern Mediterranean Background Site. *Atmos. Chem. Phys.* **2018**, *18*, 14297−14325.
(96) U.S. Environmental Protection Agency. Northeast Corridor Regional Modeling Project: Ozone and Precursor Transport in New York City and Boston During the 1980 Field Program. https://nepis.epa.gov/Exe/ZyPDF.cgi/9100LBYM.PDF?Dockey=9100LBYM.PDF (accessed Feb 4, 2022).
(97) Fiore, A. M.; Jacob, D. J.; Mathur, R.; Martin, R. V. Application of Empirical Orthogonal Functions to Evaluate Ozone Simulations with Regional and Global Models. *J. Geophys. Res.: Atmos.* **2003**, *108*, No. 4431.
(98) Kleinman, L. I.; Daum, P. H.; Imre, D. G.; Lee, J. H.; Lee, Y. N.; Nunnermacker, L. J.; Springston, S. R.; Weinstein-Lloyd, J.; Newman, L. Ozone Production in the New York City Urban Plume. *J. Geophys. Res.: Atmos.* **2000**, *105*, 14495−14511.
(99) Banta, R. M.; Senff, C. J.; White, A. B.; Trainer, M.; McNider, R. T.; Valente, R. J.; Mayor, S. D.; Alvarez, R. J.; Hardesty, R. M.; Parrish, D.; Fehsenfeld, F. C. Daytime Buildup and Nighttime Transport of Urban Ozone in the Boundary Layer during a Stagnation Episode. *J. Geophys. Res.: Atmos.* **1998**, *103*, 22519−22544.
(100) Seaman, N. L.; Stauffer, D. R.; Lario-Gibbs, A. M. A Multiscale Four-Dimensional Data Assimilation System Applied in the San Joaquin Valley during SARMAP. Part I: Modeling Design and Basic Performance Characteristics. *J. Appl. Meteorol.* **1995**, *34*, 1739−1761.

(101) Miao, Y.; Li, J.; Miao, S.; Che, H.; Wang, Y.; Zhang, X.; Zhu, R.; Liu, S. Interaction Between Planetary Boundary Layer and PM2.5 Pollution in Megacities in China: A Review. *Curr. Pollut. Rep.* **2019**, *5*, 261−271.
(102) Couillard, M. H.; Schwab, M. J.; Schwab, J. J.; Lu, C.-H.; Joseph, E.; Stutsrim, B.; Shrestha, B.; Zhang, J.; Knepp, T. N.; Gronoff, G. P. Vertical Profiles of Ozone Concentrations in the Lower Troposphere Downwind of New York City During LISTOS 2018−2019. *J. Geophys. Res.: Atmos.* **2021**, *126*, No. e2021JD035108.
(103) Vukovich, F. M. A Note on Air Quality in High Pressure Systems. *Atmos. Environ. (1967)* **1979**, *13*, 255−265.
(104) Zhang, J.; Rao, S. T.; Daggupaty, S. M. Meteorological Processes and Ozone Exceedances in the Northeastern United States During the 12-16 July 1995 Episode. *J. Appl. Meteorol.* **1998**, *37*, 776−789.
(105) Vukovich, F. M. Boundary Layer Ozone Variations in the Eastern United States and Their Association With Meteorological Variations: Long-term variations. *J. Geophys. Res.: Biogeosci.* **1994**, *99*, 16839−16850.
(106) Mazzuca, G. M.; Pickering, K. E.; New, D. A.; Dreessen, J.; Dickerson, R. R. Impact of Bay Breeze and Thunderstorm Circulations on Surface Ozone at a Site along the Chesapeake Bay 2011−2016. *Atmos. Environ.* **2019**, *198*, 351−365.
(107) Stauffer, R. M.; Thompson, A. M.; Martins, D. K.; Clark, R. D.; Goldberg, D. L.; Loughner, C. P.; Delgado, R.; Dickerson, R. R.; Stehr, J. W.; Tzortziou, M. A. Bay Breeze Influence on Surface Ozone at Edgewood, MD during July 2011. *J. Atmos. Chem.* **2015**, *72*, 335−353.
(108) Roberts, S. J.; Salawitch, R. J.; Wolfe, G. M.; Marvin, M. R.; Canty, T. P.; Allen, D. J.; Hall-Quinlan, D. L.; Krask, D. J.; Dickerson, R. R. Multidecadal Trends in Ozone Chemistry in the Baltimore-Washington Region. *Atmos. Environ.* **2022**, *285*, No. 119239.
(109) Sicard, P.; Paoletti, E.; Agathokleous, E.; Araminienė, V.; Proietti, C.; Coulibaly, F.; De Marco, A. Ozone Weekend Effect in Cities: Deep Insights for Urban Air Pollution Control. *Environ. Res.* **2020**, *191*, No. 110193.
(110) Wolff, G. T.; Kahlbaum, D. F.; Heuss, J. M. The Vanishing Ozone Weekday/Weekend Effect. *J. Air Waste Manage. Assoc.* **2013**, *63*, 292−299.
(111) De Smedt, I.; Pinardi, G.; Vigouroux, C.; Compernolle, S.; Bais, A.; Benavent, N.; Boersma, F.; Chan, K. L.; Donner, S.; Eichmann, K. U.; Hedelt, P.; Hendrick, F.; Irie, H.; Kumar, V.; Lambert, J. C.; Langerock, B.; Lerot, C.; Liu, C.; Loyola, D.; Piters, A.; Richter, A.; Rivera Cárdenas, C.; Romahn, F.; Ryan, R. G.; Sinha, V.; Theys, N.; Vlietinck, J.; Wagner, T.; Wang, T.; Yu, H.; Van Roozendael, M. Comparative Assessment of TROPOMI and OMI Formaldehyde Observations and Validation against MAX-DOAS Network Column Measurements. *Atmos. Chem. Phys.* **2021**, *21*, 12561−12593.
(112) Wang, C.; Wang, T.; Wang, P.; Rakitin, V. Comparison and Validation of TROPOMI and OMI NO_2 Observations over China. *Atmosphere* **2020**, *11*, No. 636.
(113) Goldberg, D. L.; Anenberg, S. C.; Kerr, G. H.; Mohegh, A.; Lu, Z.; Streets, D. G. TROPOMI NO_2 in the United States: A Detailed Look at the Annual Averages, Weekly Cycles, Effects of Temperature, and Correlation With Surface NO_2 Concentrations. *Earth's Future* **2021**, *9*, No. e2020EF001665.
(114) Verhoelst, T.; Compernolle, S.; Pinardi, G.; Lambert, J.-C.; Eskes, H. J.; Eichmann, K.-U.; Fjæraa, A. M.; Granville, J.; Niemeijer, S.; Cede, A.; Tiefengraber, M.; Hendrick, F.; Pazmiño, A.; Bais, A.; Bazureau, A.; Boersma, K. F.; Bognar, K.; Dehn, A.; Donner, S.; Elokhov, A.; Gebetsberger, M.; Goutail, F.; de la Mora, M.; Gruzdev, A.; Gratsea, M.; Hansen, G. H.; Irie, H.; Jepsen, N.; Kanaya, Y.; Karagkiozidis, D.; Kivi, R.; Kreher, K.; Levelt, P. F.; Liu, C.; Müller, M.; Navarro Comas, M.; Piters, A. J. M.; Pommereau, J.-P.; Portafaix, T.; Prados-Roman, C.; Puentedura, O.; Querel, R.; Remmers, J.; Richter, A.; Rimmer, J.; Rivera Cárdenas, C.; de Miguel, L.; Sinyakov, V. P.; Stremme, W.; Strong, K.; Van Roozendael, M.; Veefkind, J. P.; Wagner, T.; Wittrock, F.; Yela González, M.; Zehner, C. Ground-Based Validation of the Copernicus Sentinel-5P TROPOMI NO_2 Measurements with the NDACC ZSL-DOAS, MAX-DOAS and Pandonia Global Networks. *Atmos. Meas. Tech.* **2021**, *14*, 481−510.
(115) Vigouroux, C.; Langerock, B.; Bauer Aquino, C. A.; Blumenstock, T.; Cheng, Z.; De Mazière, M.; De Smedt, I.; Grutter, M.; Hannigan, J. W.; Jones, N.; Kivi, R.; Loyola, D.; Lutsch, E.; Mahieu, E.; Makarova, M.; Metzger, J.-M.; Morino, I.; Murata, I.; Nagahama, T.; Notholt, J.; Ortega, I.; Palm, M.; Pinardi, G.; Röhling, A.; Smale, D.; Stremme, W.; Strong, K.; Sussmann, R.; Té, Y.; van Roozendael, M.; Wang, P.; Winkler, H. TROPOMI Sentinel-5 Precursor Formaldehyde Validation Using an Extensive Network of Ground-Based Fourier-Transform Infrared Stations. *Atmos. Meas. Tech.* **2020**, *13*, 3751−3767.
(116) Zhao, X.; Griffin, D.; Fioletov, V.; McLinden, C.; Cede, A.; Tiefengraber, M.; Müller, M.; Bognar, K.; Strong, K.; Boersma, F.; Eskes, H.; Davies, J.; Ogyu, A.; Lee, S. C. Assessment of the Quality of TROPOMI High-Spatial-Resolution NO_2 Data Products in the Greater Toronto Area. *Atmos. Meas. Tech.* **2020**, *13*, 2131−2159.
(117) Griffin, D.; Zhao, X.; McLinden, C. A.; Boersma, F.; Bourassa, A.; Dammers, E.; Degenstein, D.; Eskes, H.; Fehr, L.; Fioletov, V.; Hayden, K.; Kharol, S. K.; Li, S. M.; Makar, P.; Martin, R. V.; Mihele, C.; Mittermeier, R. L.; Krotkov, N.; Sneep, M.; Lamsal, L. N.; Linden, M.; ter Geffen, J.; van Veefkind, P.; Wolde, M. High-Resolution Mapping of Nitrogen Dioxide With TROPOMI: First Results and Validation Over the Canadian Oil Sands. *Geophys. Res. Lett.* **2019**, *46*, 1049−1060.
(118) Wolfe, G. M.; Kaiser, J.; Hanisco, T. F.; Keutsch, F. N.; de Gouw, J. A.; Gilman, J. B.; Graus, M.; Hatch, C. D.; Holloway, J.; Horowitz, L. W.; Lee, B. H.; Lerner, B. M.; Lopez-Hilifiker, F.; Mao, J.; Marvin, M. R.; Peischl, J.; Pollack, I. B.; Roberts, J. M.; Ryerson, T. B.; Thornton, J. A.; Veres, P. R.; Warneke, C. Formaldehyde Production From Isoprene Oxidation Across NO_x Regimes. *Atmos. Chem. Phys.* **2016**, *16*, 2597−2610.
(119) Gonzalez Abad, G.; Souri, A. H.; Bak, J.; Chance, K.; Flynn, L. E.; Krotkov, N. A.; Lamsal, L.; Li, C.; Liu, X.; Miller, C. C.; Nowlan, C. R.; Suleiman, R.; Wang, H. Five Decades Observing Earth's Atmospheric Trace Gases Using Ultraviolet and Visible Backscatter Solar Radiation from Space. *J. Quant. Spectrosc. Radiat. Transfer* **2019**, *238*, No. 106478.
(120) Pusede, S. E.; Cohen, R. C. On the Observed Response of Ozone to NO_x And VOC Reactivity Reductions in San Joaquin Valley California 1995−Present. *Atmos. Chem. Phys.* **2012**, *12*, 8323−8339.
(121) Palmer, P. I.; Abbot, D. S.; Fu, T.-M.; Jacob, D. J.; Chance, K.; Kurosu, T. P.; Guenther, A.; Wiedinmyer, C.; Stanton, J. C.; Pilling, M. J.; Pressley, S. N.; Lamb, B.; Sumner, A. L. Quantifying the Seasonal and Interannual Variability of North American Isoprene Emissions Using Satellite Observations of the Formaldehyde Column. *J. Geophys. Res.: Atmos.* **2006**, *111*, No. D12315.
(122) Duncan, B. N.; Yoshida, Y.; Damon, M. R.; Douglass, A. R.; Witte, J. C. Temperature Dependence of Factors Controlling Isoprene Emissions. *Geophys. Res. Lett.* **2009**, *36*, No. L05813.
(123) He, H.; Liang, X. Z.; Sun, C.; Tao, Z.; Tong, D. Q. The Long-Term Trend and Production Sensitivity Change in the Us Ozone Pollution From Observations and Model Simulations. *Atmos. Chem. Phys.* **2020**, *20*, 3191−3208.
(124) Singh, S.; Kavouras, I. G. Trends of Ground-Level Ozone in New York City Area during 2007−2017. *Atmosphere* **2022**, *13*, No. 114.
(125) Zhu, Q.; Laughner, J. L.; Cohen, R. C. Estimate of OH Trends over One Decade in North American Cities. *Proc. Natl. Acad. Sci. U.S.A.* **2022**, *119*, No. e2117399119.
(126) Steinemann, A. Volatile Emissions from Common Consumer Products. *Air Qual., Atmos. Health* **2015**, *8*, 273−281.
(127) McDonald, B. C.; De Gouw, J. A.; Gilman, J. B.; Jathar, S. H.; Akherati, A.; Cappa, C. D.; Jimenez, J. L.; Lee-Taylor, J.; Hayes, P. L.; McKeen, S. A.; Cui, Y. Y.; Kim, S. W.; Gentner, D. R.; Isaacman-VanWertz, G.; Goldstein, A. H.; Harley, R. A.; Frost, G. J.; Roberts, J. M.; Ryerson, T. B.; Trainer, M. Volatile Chemical Products Emerging

as Largest Petrochemical Source of Urban Organic Emissions. *Science* **2018**, *359*, 760−764.
(128) Gkatzelis, G. I.; Coggon, M. M.; McDonald, B. C.; Peischl, J.; Gilman, J. B.; Aikin, K. C.; Robinson, M. A.; Canonaco, F.; Prevot, A. S. H.; Trainer, M.; Warneke, C. Observations Confirm That Volatile Chemical Products Are a Major Source of Petrochemical Emissions in U.S. Cities. *Environ. Sci. Technol.* **2021**, *55*, 4332−4343.
(129) Coggon, M. M.; Gkatzelis, G. I.; McDonald, B. C.; Gilman, J. B.; Schwantes, R. H.; Abuhassan, N.; Aikin, K. C.; Arendd, M. F.; Berkoff, T. A.; Brown, S. S.; Campos, T. L.; Dickerson, R. R.; Gronoff, G.; Hurley, J. F.; Isaacman-Vanwertz, G.; Koss, A. R.; Li, M.; McKeen, S. A.; Moshary, F.; Peischl, J.; Pospisilova, V.; Ren, X.; Wilson, A.; Wu, Y.; Trainer, M.; Warneke, C. Volatile Chemical Product Emissions Enhance Ozone and Modulate Urban Chemistry. *Proc. Natl. Acad. Sci. U.S.A.* **2021**, *118*, No. e2026653118.
(130) Furdyna, P.; Felton, D.Picarro G2307 Analyzer Updates [PowerPoint Slides]. https://www.nescaum.org/documents/listos/1300-4-listos-picarro_furdyna-20211014.pdf (accessed March 31, 2022).

https://doi.org/10.1021/acs.est.2c02972
Environ. Sci. Technol. 2022, 56, 15312−15327